Crystallography of optical lattices

K. I. Petsas, A. B. Coates,* and G. Grynberg
Laboratoire Kastler Brossel,† Département de Physique de l'Ecole Normale Supérieure, 24 rue Lhomond, 75231 Paris Cedex 05, France
(Received 7 July 1994)

We present a theoretical study of three- and four-beam configurations that generalize, in the two-dimensional (2D) and three-dimensional (3D) cases, the well-known 1D lin ⊥ lin (two counterpropagating beams having crossed linear polarizations) and magnetic-assisted Sisyphus effect cooling schemes. It is shown how the Bravais lattice is determined from the propagation directions of the laser beams while the basis is associated with the polarizations of the incident waves. The optical potentials are calculated for a $J_g=\frac{1}{2}\rightarrow J_e=\frac{3}{2}$ transition for a variety of angular and polarization configurations and some of the characteristics of the atomic motion inside a single micrometer-sized potential well are predicted.

PACS number(s): 32.80.Pj, 42.65.−k, 61.50.Em

I. INTRODUCTION

It was recently shown that atoms can be cooled and trapped in a periodic lattice of micrometer-sized potential wells originating from the interference of a number of incident beams which are nearly resonant for a transition coupling the ground state (g,J_g) to an excited state (e,J_e) [1]. The binding energy of the atoms in these wells is associated with the light shift [2] of the ground-state Zeeman sublevels and the atoms are cooled by the Sisyphus effect [3]. The first experiments involving these lattices explored one-dimensional (1D) configurations [4–7]. Following the suggestion of Castin and Dalibard [8], the first beam configuration that was experimentally studied [4,5] was the 1D lin⊥lin configuration, in which two beams having crossed linear polarizations propagate in opposite directions. In particular, the vibrational frequency of alkali-metal atoms in the bottom of a potential well was measured by stimulated Raman spectroscopy by Verkerk *et al.* [4] and by spontaneous Raman spectroscopy by Jessen *et al.* [5]. Later experiments showed that a similar trapping occurs in the case of the 1D magnetic-assisted Sisyphus effect (MASE) configuration [6,7]. In these latter experiments, the counterpropagating beams are circularly polarized and the cooling arises from the mixing of the Zeeman sublevels due to a small transverse magnetic field [9]. The experiments suggested that the design of a two-dimensional (2D) or three-dimensional (3D) lattice should obey the following two rules: first, the field geometry should provide an efficient multidimensional Sisyphus cooling, and second, the light polarization at the bottom of the potential well should be circular to obtain long trapping times in the wells and narrow vibrational transitions [10]. This is because an atom having a strongly confined external wave function (Lamb-Dicke regime) has only a very small probability of escaping a potential well associated with a Zeeman sublevel for which $|m_g|=J_g$ (m_g being the magnetic quantum number) by absorbing a photon of the minority circular polarization. In fact, an optical lattice may be achieved in conditions where this second rule is not fulfilled, but the observation of Raman transitions between vibrational states is expected to be more difficult because of the absence of the localization narrowing in the Lamb-Dicke regime. The lattices for which atoms are localized in potential wells for which $|m_g|=J_g$ can be split into two categories. The first category corresponds to lattices in which the atoms have the same probability of occupying a well associated with $m_g=J_g$ as a well for which $m_g=-J_g$. In this case, the two opposite orientations of the magnetic moment are expected to be found with the same probability and these lattices will be described as *antiferromagnetic.* For example, the 1D lin⊥lin configuration gives rise to an antiferromagnetic lattice [4]. In the second category, trapping is only expected in wells corresponding to a single magnetic quantum number (either $m_g=J_g$ or $-J_g$). The localized atoms have the same magnetic moment; these lattices are called *ferromagnetic.* The 1D MASE configuration leads to a ferromagnetic lattice [7].

The first observation of a 2D optical lattice was performed by Hemmerich and Hänsch [11], who used two orthogonal standing waves having a well-defined phase difference. The locking of this phase is important in order to achieve a lattice in which the polarization is circular at the bottom of the potential wells. In fact, Raman transitions between vibrational levels were observed only around this particular value of the phase. Soon after, another type of 2D lattice was obtained by Grynberg *et al.* by using three traveling waves [12]. In this case, the maps of the potential and of the light polarization are independent of the phases of the beams. A change in the

*Present address: Department of Physics, the University of Queensland, QLD 4072 Australia.
†Laboratoire associé au Centre National de la Recherche Scientifique et à l'Université Pierre et Marie Curie.

phase just results in a translation of the lattice. The same idea was applied to the three-dimensional case and a 3D optical lattice was observed using four traveling waves that do not propagate in the same plane [12]. Although these lattices are experimentally quite interesting because of their lack of sensitivity to phase fluctuations, 3D lattices using more than four incident traveling waves can also be efficient for trapping atoms provided that the relative phase is controlled, as shown by Hemmerich, Zimmermann, and Hänsch, who realized a lattice using three mutually orthogonal standing waves [13]. In fact, even in the case where the lattice is designed with the minimum number of beams (three in 2D, four in 3D), there are many possibilities for the choice of the beam polarizations and directions of propagation. One of the simplest methods for building a 3D configuration is to start from one of the well-known 1D field configurations [lin⊥lin, MASE, σ^+-σ^- (two counterpropagating beams with orthogonal circular polarizations) [3,14]] and to split the incident beams. Such a 3D lattice, obtained by splitting the two counterpropagating beams of the 1D lin⊥lin configuration into two different planes, was recently demonstrated [15]. It is the aim of this paper to generalize this approach and to present some lattice configurations that can be achieved using this method.

Following a suggestion of [12], we first present in Sec. II a simple method for determining the spatial periodicity of an optical lattice from the characteristics of the reciprocal lattice whose primitive cell is shown to be generated by vectors of the type $\mathbf{k}_i-\mathbf{k}_j$ (where $\mathbf{k}_i$ is the wave vector of an incident field). This method is then applied to determine the lattice structure for several beam configurations. We consider in Secs. III and IV several possible 2D and 3D extensions of the lin⊥lin and the MASE configurations. As with the initial 1D configurations, these 2D and 3D configurations are expected to lead to atomic localization in a range of geometrical parameters for the incident beams that are studied. We also predict the characteristics of the vibrational motion in the potential wells for the case of a transition connecting a ground state of angular momentum $J_g=\frac{1}{2}$ to an excited state for which $J_e=\frac{3}{2}$. Using the same approach, we study in the Appendix a 3D generalization of the σ^+-σ^- configuration (although atomic localization is not expected, the potential and the light polarization exhibit spatial periodicity). In particular, we study the conditions under which the 1D orientational cooling can be preserved along well-defined wires in the 3D case.

II. SPATIAL PERIODICITY

To understand the geometrical characteristics of an optical lattice we have to determine its spatial periodicity and the basis inside one unit cell. The determination of the basis means to find the potential wells and the light polarization at the bottoms of the wells. The incident beams are characterized by their directions of propagation $\mathbf{k}_i$ and their polarizations $\mathbf{e}_i$. In fact, as shown in Sec. II A, the spatial periodicity depends only on the wave vectors $\mathbf{k}_i$, whereas the basis also depends on $\mathbf{e}_i$. Thus modifying the light polarization while leaving the $\mathbf{k}_i$ fixed changes the basis, but not the lattice in the crystallographic meaning.

A. Reciprocal lattice

The reciprocal lattice ia a useful concept in solid-state physics, particularly for the determination of the Bragg scattering directions. There is a unique correspondence between the direct and reciprocal spaces and therefore the direct lattice can be determined from a knowledge of the reciprocal lattice. Using a remark made in [12], we wish to show that the determination of the reciprocal lattice is particularly straightforward.

If we consider a weak probe beam having a wave vector $\mathbf{k}_p$ incident on the lattice, we know from solid-state physics that the possible directions for Bragg scattering are given by [16]

$$\mathbf{k}_s=\mathbf{k}_p+\mathbf{K} , \tag{1}$$

where $\mathbf{k}_s$ is the wave vector of the scattered photon, $|\mathbf{k}_s|=|\mathbf{k}_p|$, and $\mathbf{K}$ is a vector of the reciprocal lattice.

From a nonlinear-optics point of view, a coherent emission occurs in directions for which multiwave mixing is phase matched. In these directions, there is no momentum transfer from the field to the atoms. The change in momentum of the scattered photon should be balanced by a redistribution of photons in the lattice beams. For example, a photon absorption from the beam $\mathbf{k}_1$ followed by a stimulated emission into the beam $\mathbf{k}_2$ involves a change of momentum equal to $\hbar(\mathbf{k}_1-\mathbf{k}_2)$. More generally, any redistribution process among N beams involves a change of the atomic momentum $\mathbf{P}$ equal to

$$\mathbf{P}=\sum_{l=2}^{N} n_l\hbar(\mathbf{k}_1-\mathbf{k}_l) , \tag{2}$$

where the n_l are integers which may be negative, positive, or null [17]. Since the modification of the atomic momentum in a multiwave mixing process is

$$\mathbf{P}=\hbar(\mathbf{k}_p-\mathbf{k}_s)+\sum_{l=2}^{N} n_l\hbar(\mathbf{k}_1-\mathbf{k}_l)=\mathbf{0} , \tag{3}$$

one concludes from a comparison between (1) and (3) that $(\mathbf{k}_1-\mathbf{k}_2),(\mathbf{k}_1-\mathbf{k}_3)$, etc. are basis vectors for the reciprocal lattice. In the case of a 2D lattice, the reciprocal lattice is generated by the two vectors $(\mathbf{k}_1-\mathbf{k}_2)$ and $(\mathbf{k}_1-\mathbf{k}_3)$. In the case of a 3D lattice, the vectors $(\mathbf{k}_1-\mathbf{k}_2)$, $(\mathbf{k}_1-\mathbf{k}_3)$, and $(\mathbf{k}_1-\mathbf{k}_4)$ are primitive vectors of the reciprocal lattice. Examples of the determination of 2D and 3D lattice structures using this method will be presented in Sec. II C, but we wish first to comment on the field configurations that involve more than the minimum number of beams.

B. Lattices and molasses

In the lattice configurations studied by Hemmerich and co-workers [11,13], the vectors $(\mathbf{k}_1-\mathbf{k}_2),\ldots,(\mathbf{k}_1-\mathbf{k}_N)$

can be expressed, in the 3D case, as linear combinations of *three* vectors with integer coefficients, while the 2D case requires only *two* vectors. For example, in the 2D case where $\mathbf{k}_2=-\mathbf{k}_1$ and $\mathbf{k}_4=-\mathbf{k}_3$, one can take $(\mathbf{k}_2-\mathbf{k}_1)$ and $(\mathbf{k}_3-\mathbf{k}_1)$ as basis vectors because

$$\mathbf{k}_4-\mathbf{k}_1=-(\mathbf{k}_3-\mathbf{k}_2)=(\mathbf{k}_2-\mathbf{k}_1)-(\mathbf{k}_3-\mathbf{k}_1)\ . \tag{4}$$

As far as spatial periodicity is concerned, there is no difference between a 3D molasses for which $\mathbf{k}_2=-\mathbf{k}_1$, $\mathbf{k}_4=-\mathbf{k}_3$, and $\mathbf{k}_6=-\mathbf{k}_5$ and the Hemmerich-Hänsch lattice because they both correspond to the same reciprocal lattice. Of course, the spatial distribution of the potential wells and of the light polarization depends on the relative phases of the beams and on their respective polarizations, but the translational symmetries are obviously the same in both cases [18].

C. Splitting a one-dimensional configuration

We now consider a 1D configuration consisting of two counterpropagating beams propagating along the z direction [Fig. 1(a)] and show how 2D and 3D lattices can be built by splitting one or two of the beams of this configuration.

1. Two-dimensional configurations

We consider the configuration where the beam propagating in the $-\mathbf{k}$ direction of Fig. 1(a) is split into two beams. Although it is not necessary that these two beams be symmetric with respect to Oz in order to design an optical lattice, we restrict the study here to this simpler case [Fig. 1(b)]. The wave vectors of the three beams are respectively given by

$$\begin{aligned}\mathbf{k}_1&=k\mathbf{e}_z\ ,\\ \mathbf{k}_2&=k\sin(\vartheta)\mathbf{e}_y-k\cos(\vartheta)\mathbf{e}_z\ ,\\ \mathbf{k}_3&=-k\sin(\vartheta)\mathbf{e}_y-k\cos(\vartheta)\mathbf{e}_z\ ,\end{aligned} \tag{5}$$

where $0<\vartheta<\pi$. Note that it is possible to consider a lattice for which $\pi/2<\vartheta<\pi$ [Fig. 1(c)]. Although the atom will always experience a radiation pressure along Oz for this field configuration, the reactive force associated with the light shift should be dominant for sufficiently large values of $|\Delta|/\Gamma$ ($\Delta=\omega_L-\omega_0$ being the laser detuning from resonance and Γ being the natural width of the excited state).

In the following we use the shorter notations:

$$K_\perp=\frac{2\pi}{\lambda_\perp}=k\sin\vartheta,\quad K_\parallel=\frac{2\pi}{\lambda_\parallel}=k\frac{(1+\cos\vartheta)}{2}\ . \tag{6}$$

The results of Sec. II A permit us to find the following primitive translation vectors of the reciprocal lattice:

$$\begin{aligned}\mathbf{a}_1^*&=\mathbf{k}_2-\mathbf{k}_1=K_\perp\mathbf{e}_y-2K_\parallel\mathbf{e}_z\ ,\\ \mathbf{a}_2^*&=\mathbf{k}_2-\mathbf{k}_3=2K_\perp\mathbf{e}_y\ .\end{aligned} \tag{7}$$

Then, using the simple algebraic transformation defined by $\mathbf{a}_i\cdot\mathbf{a}_j^*=2\pi\delta_{ij}$ [16], we deduce the vectors $\mathbf{a}_i$ that generate the primitive cell of the direct lattice:

$$\mathbf{a}_1=-\frac{\lambda_\parallel}{2}\mathbf{e}_z,\quad \mathbf{a}_2=\frac{\lambda_\perp}{2}\mathbf{e}_y+\frac{\lambda_\parallel}{4}\mathbf{e}_z\ . \tag{8}$$

These vectors make an angle that is given by $\cos(\mathbf{a}_1,\mathbf{a}_2)=-\sin(\vartheta)/\sqrt{2(1+\cos\vartheta)}$. It can be seen that the 2D optical lattice is generally centered rectangular. In the particular case where $\vartheta=60°$, the two primitive translation vectors of the direct space have equal lengths and make an angle of 120° leading to a hexagonal lattice. This geometry was used in the experiment performed by Grynberg *et al.* [12]. In Figs. 2(a) and 2(b) we give illustrations of the optical lattice which is obtained for the 2D extension of the lin⊥lin configuration, which will be discussed in Sec. III.

2. Three-dimensional umbrellalike configurations

To obtain a 3D configuration, one can split one of the beams of the 1D configuration into three beams [Fig. 1(d)]. Here again, although it is not necessary to have a symmetric splitting, we only consider the case where the three wave vectors make a common angle ϑ with the Oz axis ($0<\vartheta<\pi$). Taking the azimuthal angles of the three beams to be $\phi_n=2n\pi/3$, where $n=0,1,2$, the wave vectors of the four cooling beams are

$$\begin{aligned}\mathbf{k}_n&=-k\sin\vartheta\cos(\phi_n)\mathbf{e}_x-k\sin\vartheta\sin(\phi_n)\mathbf{e}_y\\ &\quad+k\cos(\vartheta)\mathbf{e}_z,\quad \mathbf{k}_3=-k\mathbf{e}_z\ .\end{aligned} \tag{9}$$

Using the notations $K_\parallel$ and $K_\perp$ introduced in Eq. (6), we find that a primitive unit cell of the reciprocal lattice can be generated by the following three vectors:

$$\mathbf{a}_1^*=\mathbf{k}_0-\mathbf{k}_3=-K_\perp\mathbf{e}_x+2K_\parallel\mathbf{e}_z\ , \tag{10a}$$

$$\mathbf{a}_2^*=\mathbf{k}_1-\mathbf{k}_3=\tfrac{1}{2}K_\perp\mathbf{e}_x-\frac{\sqrt{3}}{2}K_\perp\mathbf{e}_y+2K_\parallel\mathbf{e}_z\ , \tag{10b}$$

$$\mathbf{a}_3^*=\mathbf{k}_2-\mathbf{k}_3=\tfrac{1}{2}K_\perp\mathbf{e}_x+\frac{\sqrt{3}}{2}K_\perp\mathbf{e}_y+2K_\parallel\mathbf{e}_z\ . \tag{10c}$$

These three vectors have the same length and make the same angle α with each other, whatever the value of ϑ. As a result, the reciprocal lattice is trigonal. The expression of α as a function of ϑ is given by

$$\cos\alpha=\frac{1}{2}\left[\frac{3\cos^2\vartheta+4\cos\vartheta+1}{2+2\cos\vartheta}\right]\ . \tag{11}$$

In the particular case where $\cos\vartheta=\frac{1}{3}$, one finds from (11) that $\cos\alpha=\frac{1}{2}$ and the primitive cell of the reciprocal lattice corresponds to a conventional face-centered-cubic one. When $\cos\alpha=-\frac{1}{3}$, which corresponds to $\cos\vartheta=-\frac{7}{9}$, the reciprocal lattice is cubic body centered.

This discussion, transposed into direct space, permits us to deduce the nature of the optical lattice. Hence, in the most general case, the lattice is trigonal (R). A cubic body-centered (I) structure is obtained if the beams are propagating along the threefold symmetry axes of a regular tetrahedron (i.e., when $\cos\vartheta=\frac{1}{3}$). Note that in this case, the propagation directions of the four beams are identical to the directions used in the experiment of Ref. [12]. Finally, a geometry for which $\cos\vartheta=-\frac{7}{9}$ leads to a

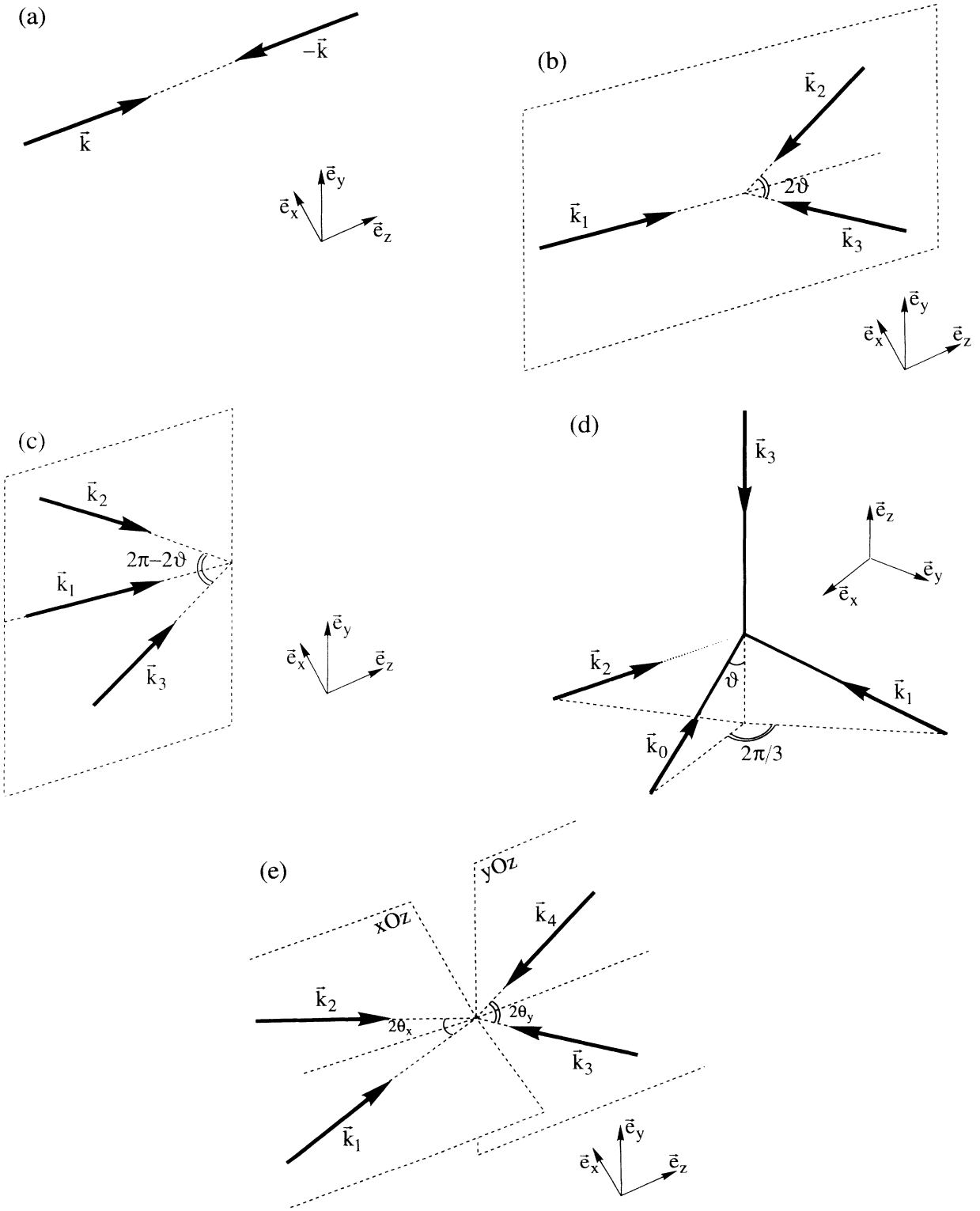

FIG. 1. Splitting a one-dimensional configuration to generate 2D or 3D optical lattices. The bases of these lattices will result from the particular polarizations of the beams, but the propagation directions presented here suffice to determine the nature of the Bravais lattice. (a) The initial 1D configuration: two identical laser beams counterpropagating along the z direction. (b) Two-dimensional configurations: one of the beams is split into two beams, of which the propagation directions are contained in the yOz plane making an angle ϑ ($0<\vartheta<\pi/2$) with the z axis. (c) Same as (b), but for $\pi/2<\vartheta$. (d) Three-dimensional *umbrellalike* configurations: one of the beams is split into three beams. The propagation directions of the three resulting waves each make an angle ϑ with Oz and have azimuthal angles given by $\phi_n=2n\pi/3$ (where ϕ_n is associated with the beam $\mathbf{k}_n$, $n=0,1,2$). (e) Three-dimensional configurations resulting from a symmetric splitting: one of the initial beams is divided into two beams that propagate in the xOz plane making an angle θ_x with the z axis, while the other one is split into two beams that propagate in the yOz plane making an angle θ_y with Oz.

face-centered-cubic (F) lattice. These results are illustrated in Figs. 3(a) and 3(b) in the particular case of the lin⊥lin polarization scheme, which we will discuss subsequently.

3. *Three-dimensional configurations resulting from splitting both beams*

Instead of keeping one beam of the 1D configuration unchanged and splitting the other one into three beams, it is also possible to split each of the two counterpropagating beams into two beams. Here again, we restrict our study to a case of relatively high symmetry where one beam is split into two beams propagating in the xOz plane and making an angle $2\theta_x$, while the other beam is split into two beams propagating in the yOz plane and making an angle $2\theta_y$. The beam configuration being symmetric with respect to xOz and yOz, the four incident wave vectors are, respectively,

$$\mathbf{k}_1 = k\sin(\theta_x)\mathbf{e}_x + k\cos(\theta_x)\mathbf{e}_z\ , \qquad \mathbf{k}_2 = -k\sin(\theta_x)\mathbf{e}_x + k\cos(\theta_x)\mathbf{e}_z\ ; \tag{12a}$$

$$\mathbf{k}_3 = k\sin(\theta_y)\mathbf{e}_y - k\cos(\theta_y)\mathbf{e}_z\ , \qquad \mathbf{k}_4 = -k\sin(\theta_y)\mathbf{e}_y - k\cos(\theta_y)\mathbf{e}_z\ . \tag{12b}$$

In the following we use the shorter notations

$$K_x = \frac{2\pi}{\lambda_x} = k\sin\theta_x, \quad K_y = \frac{2\pi}{\lambda_y} = k\sin\theta_y\ , \qquad K_\pm = \frac{2\pi}{\lambda_\pm} = k\left[\frac{\cos\theta_x \pm \cos\theta_y}{2}\right]\ . \tag{13}$$

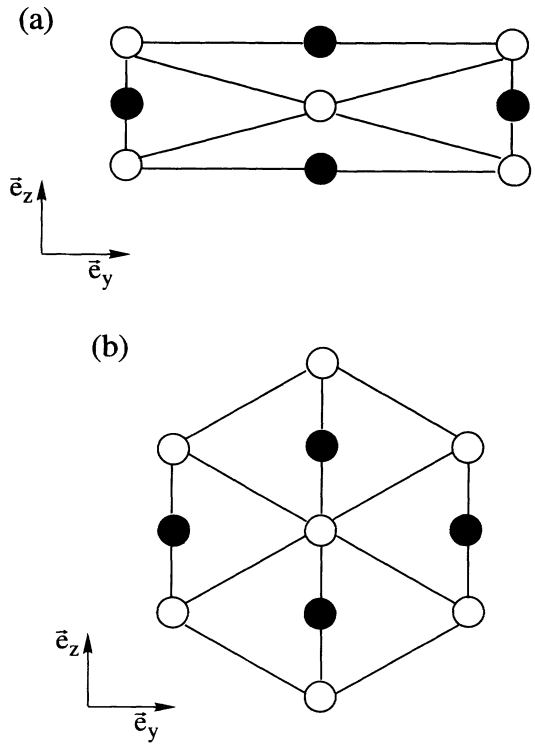

FIG. 2. Conventional unit cells of 2D optical lattices resulting from the beam geometries of Figs. 1(b) and 1(c). The white and gray dots indicate two different types of *micrometer-sized potential wells* associated with opposite circular polarizations. These lattices correspond to the 2D generalization of the lin⊥lin scheme that is presented in Sec. III: one of the beams of Fig. 1(b) [or 1(c)] is x polarized, whereas the two counterpropagating beams are linearly polarized in the yOz plane. The particular basis, as well as the *antiferromagnetic order,* results from this choice of polarizations for the cooling beams. (a) $\vartheta \neq 60°$: the optical lattice is centered rectangular. (b) Particular case where $\vartheta = 60°$: the lattice is hexagonal (this beam geometry was used in the experiment of Ref. [12], but the polarizations of the three beams were different, leading to a different lattice basis).

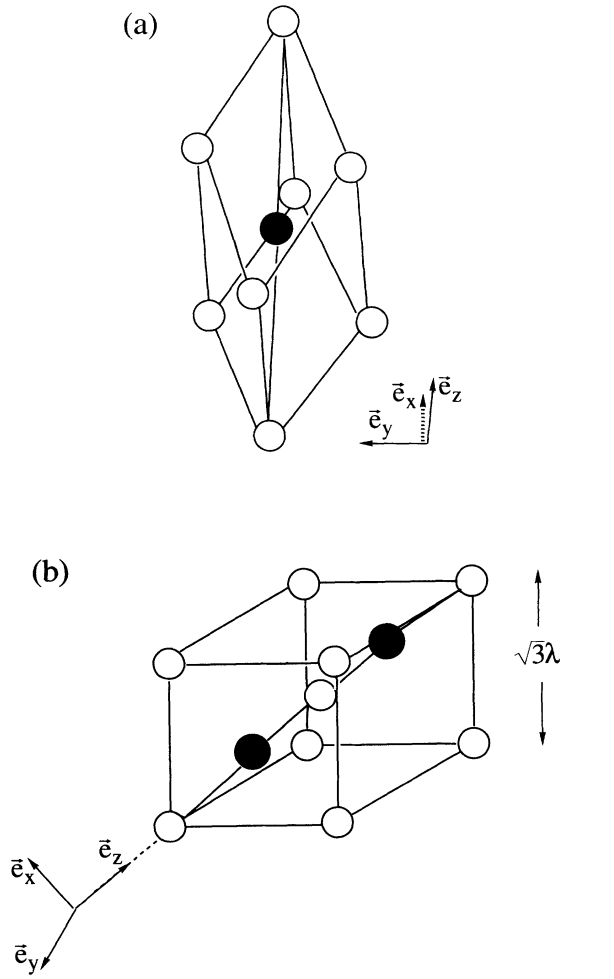

FIG. 3. Conventional unit cells of 3D optical lattices resulting from the beam geometry of Fig. 1(d). As for Fig. 2, the white and gray dots indicate two different types of sites associated with opposite circular polarizations at the bottoms of the potential wells. The basis of the lattice is associated with the 3D umbrellalike generalization of the lin⊥lin configuration that is presented in Sec. III. (a) Trigonal lattice obtained in the general case. The diagonal of the rhombohedral unit cell lies along the z axis. (b) Body-centered-cubic lattice, obtained in the particular case where $\cos\vartheta = \frac{1}{3}$. The diagonal of the cube lies along the Oz direction.

Following the discussion of Sec. II A, primitive translations of reciprocal space can be generated by

$$\mathbf{a}_1^* = \mathbf{k}_2 - \mathbf{k}_4 = -K_x \mathbf{e}_x + K_y \mathbf{e}_y + 2K_+ \mathbf{e}_z \ , \tag{14a}$$

$$\mathbf{a}_2^* = \mathbf{k}_1 - \mathbf{k}_3 = K_x \mathbf{e}_x - K_y \mathbf{e}_y + 2K_+ \mathbf{e}_z \ , \tag{14b}$$

$$\mathbf{a}_3^* = \mathbf{k}_3 - \mathbf{k}_2 = K_x \mathbf{e}_x + K_y \mathbf{e}_y - 2K_+ \mathbf{e}_z \ . \tag{14c}$$

Generally, Eqs. (14) express the primitive unit cell of a centered orthorhombic lattice in reciprocal space. In the particular cases where $\theta_x = \theta_y$, this lattice is centered tetragonal. Furthermore, the lattice is body-centered cubic for $\cos\theta_x = \cos\theta_y = 1/\sqrt{5}$ and face-centered cubic for $\cos\theta_x = \cos\theta_y = 1/\sqrt{3}$ [19].

These considerations in reciprocal space permit us to infer the structure of the direct lattice. Thus, in the most general case, the optical lattice is face-centered orthorhombic (F). When $\theta_x = \theta_y$, the lattice is simple tetragonal (P). In addition, for $\cos\theta_x = \cos\theta_y = 1/\sqrt{5}$ and $\cos\theta_x = \cos\theta_y = 1/\sqrt{3}$, face-centered-cubic ($F$) and body-centered-cubic (I) lattices are respectively obtained [the case of the lin⊥lin configurations is illustrated in Figs. 4(a) and 4(b)].

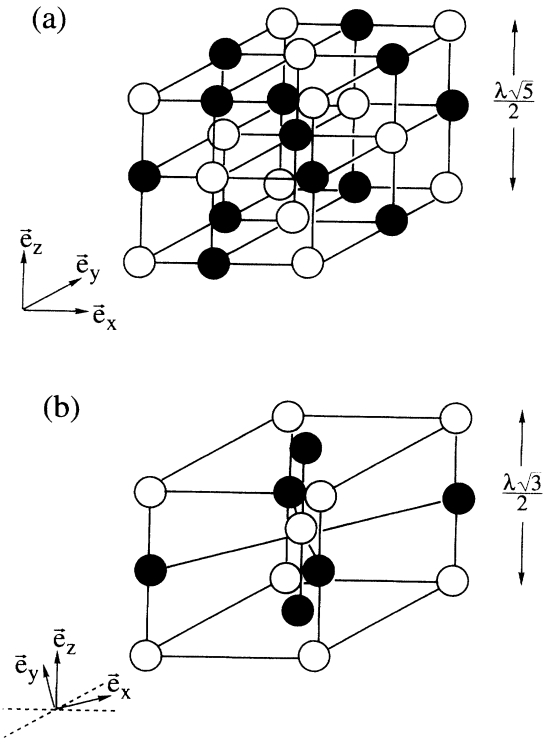

FIG. 4. Particular cases of the 3D lattice obtained from a symmetrical splitting of the 1D configuration [Fig. 1(e)]. We show the conventional unit cell of the lattice. White and gray dots indicate two different types of sites associated with opposite circular polarizations at the bottoms of the potential wells. The polarizations of the beams correspond to a 3D generalization of the lin⊥lin configuration, described in detail in Sec. III B 1 (or in Sec. III B 2). (a) Face-centered-cubic lattice obtained for $\theta_x = \theta_y = \arccos(1/\sqrt{5})$. The lattice has a NaCl crystal-like structure for the particular choice of polarizations that is made in Sec. III B 1 (or Sec. III B 2). (b) Body-centered-cubic lattice obtained for $\theta_x = \theta_y = \arccos(1/\sqrt{3})$.

III. GENERALIZATION OF THE lin⊥lin CONFIGURATION

In this section we present a two-dimensional and a few three-dimensional generalizations of the well-known 1D lin⊥lin configuration [3]. This field configuration consists of two traveling waves, linearly cross polarized and propagating in opposite directions along the Oz axis. The directions of the field polarizations are Ox and Oy. The optical potential is calculated for the simple case of a $J_g = \frac{1}{2} \rightarrow J_e = \frac{3}{2}$ transition. Even though actual experiments are often performed using more complicated transitions, it appears that the basic mechanisms can often be understood from calculations which assume this simpler transition. Because of their analytical complexities, we do not give the general expressions of the optical potential, but we plot some of its principal sections; these permit us to understand the characteristics of the atomic motion. The form of the electric field, resulting from the combination of the cooling beams, is required for calculations not only of the optical potential but also, in the case of probe transmission spectroscopy, of the probe transmission spectrum. We also give the amounts of the σ^+, σ^-, and π components of the light in the vicinity of the minima of the optical potential. These quantities permit us to find the vibrational frequencies and to evaluate the relaxation rates for the atoms localized near the bottom of the potential wells.

The principle of the calculation is as follows. We express the total electric field in Cartesian coordinates as

$$\mathbf{E}(\mathbf{r}) = \tfrac{1}{2}[E_x(\mathbf{r})\mathbf{e}_x + E_y(\mathbf{r})\mathbf{e}_y + E_z(\mathbf{r})\mathbf{e}_z] e^{-i\omega_L t} + \text{c.c.} \ , \tag{15a}$$

where ω_L is the common frequency of the four beams, or in circular coordinates as

$$\mathbf{E}(\mathbf{r}) = \tfrac{1}{2}[E_+(\mathbf{r})\boldsymbol{\varepsilon}_1 + E_-(\mathbf{r})\boldsymbol{\varepsilon}_{-1} + E_z(\mathbf{r})\boldsymbol{\varepsilon}_0] e^{-i\omega_L t} + \text{c.c.} \ , \tag{15b}$$

where $\boldsymbol{\varepsilon}_{\pm 1} = \mp(\mathbf{e}_x \pm i\mathbf{e}_y)/\sqrt{2}$, $\boldsymbol{\varepsilon}_0 = \mathbf{e}_z$, are the circular basis unit vectors. By introducing the local polarization $\boldsymbol{\varepsilon}(\mathbf{r})$ and the local amplitude $E_L(\mathbf{r})$ of the laser field, $\mathbf{E}(\mathbf{r})$ can also be written as

$$\mathbf{E}(\mathbf{r}) = \tfrac{1}{2} E_L(\mathbf{r}) e^{-i\omega_L t} \boldsymbol{\varepsilon}(\mathbf{r}) + \text{c.c.} \tag{16}$$

The light shifts of the ground-state sublevels are the eigenvalues of the light-shift operator [20]

$$\hat{\Lambda}(\mathbf{r}) = [\boldsymbol{\varepsilon}^*(\mathbf{r}) \cdot \hat{\mathbf{d}}^-][\boldsymbol{\varepsilon}(\mathbf{r}) \cdot \hat{\mathbf{d}}^+] \frac{\Delta}{4\hbar \left[\frac{\Gamma^2}{4} + \Delta^2 \right]} D^2 E_L^2(\mathbf{r}) \ , \tag{17}$$

where D is the matrix element of the electric dipole moment operator between the ground and excited states for a Clebsch-Gordan coefficient equal to 1. The matrix elements of the reduced dipole operator $\hat{d}_q^{\pm} = \boldsymbol{\varepsilon}_q \cdot \hat{\mathbf{d}}^{\pm}$ ($q = 0, \pm 1$) are the Clebsch-Gordan coefficients for the transition considered. The optical potential is thus ob-

tained from the diagonalization of $\hat{\Lambda}(\mathbf{r})$. After having found the minima of the potential, we study the light polarization in their vicinities.

It should be noted that we neglect the radiation pressure in the following calculations. For the 2D and 3D beam geometries considered below, and contrary to the 1D case, the total radiation pressure does not cancel everywhere. However, the reactive part of the atom-field coupling (light-shift operator) is larger than the dissipative part, which involves radiation pressure, by a factor of the order of $|\Delta|/\Gamma$. Because most experiments [12,15] are done in a range where $|\Delta|/\Gamma \gg 1$, a first approach to treating these lattices in terms of the optical potential alone seems reasonable. Such an approximation is probably good inside the potential wells and permits us to predict the vibrational motion.

A. Example of a 2D lattice

Starting from the usual 1D lin⊥lin configuration, there are two obvious solutions for splitting the beams, following Fig. 1(b). The first one consists in splitting the y-polarized beam into two y-polarized beams propagating in the xOz plane and making an angle 2ϑ, the x-polarized beam being unchanged. The second solution consists in splitting the y-polarized beam into two beams propagating in the yOz plane and linearly polarized in this plane, the x-polarized beam being unchanged.

The first case is particularly simple because the field polarization is always perpendicular to Oz. To obtain a field which is circularly polarized at the bottom of the potential wells, we choose the following amplitudes: for the field polarized along the x direction $\mathcal{E}_1 = E_0$ and for the y-polarized beams $\mathcal{E}_2 = \mathcal{E}_3 = E_0/2$. One obtains in this case an antiferromagnetic lattice (because there are as many σ^+ as σ^- potential wells having the same depth) whose spatial periodicity has been described in Sec. II C 1.

We wish to discuss in more detail the second example because it demonstrates the phenomenon of the modification of the topography of the potential which occurs for particular propagation directions. This phenomenon occurs in many 3D examples. The amplitudes of the incident waves are chosen to be $\mathcal{E}_1 = E_0$ for the x-polarized wave propagating along $\mathbf{k}_1$ [see Eq. (5)] and $\mathcal{E}_{2,3} = E_0/2\cos\vartheta$ for the two waves polarized in the yOz plane propagating along $\mathbf{k}_2$ and $\mathbf{k}_3$. This choice of the relative amplitudes of the three waves permits us to obtain purely circular polarized light at the bottoms of the potential wells. The field components in the circular polarization basis introduced in Eq. (15b) are therefore equal to

$$E_{\pm}(\mathbf{r}) = \frac{E_0}{\sqrt{2}} e^{ikz}[\cos(K_\perp y) e^{-2iK_\parallel z} \mp 1] , \tag{18a}$$

$$E_z(\mathbf{r}) = -E_0 e^{ikz} \sin(K_\perp y) e^{-2iK_\parallel z} \tan\vartheta . \tag{18b}$$

It should be noted that the values of the relative phases of the cooling beams have been chosen so as to simplify the form of Eqs. (18). A change in these phases would result in a global spatial translation of the light shifts, so that the topography of the optical potential would be left unchanged.

Unlike the 1D case the light-shift operator is not diagonal in the ground-state Zeeman sublevel basis $|g, m_z = \pm\frac{1}{2}\rangle$. We carry out the calculation of the optical potential $V_{\text{opt}}(y,z)$ by diagonalization of $\hat{\Lambda}(\mathbf{r})$. The topography of the potential is illustrated in Fig. 5 for the case of $\vartheta = 20°$. The potential minima, represented by the white zones of the figure, are located at

$$\mathbf{R}_{m,n} = m\frac{\lambda_\perp}{2}\mathbf{e}_y + n\frac{\lambda_\parallel}{4}\mathbf{e}_z \quad (m,n \text{ integers}) . \tag{19a}$$

More explicitly, we can distinguish two kinds of sites with respect to the light polarization: $\mathbf{R}^{(-)}_{m,n}$ corresponding to $m+n$ even and $\mathbf{R}^{(+)}_{m,n}$ for odd values of $m+n$. As can be seen from Eqs. (18a) and (18b), the light is, respectively, σ^- and σ^+ circularly polarized at these points. The basis of the optical lattice consists of two adjacent minima long the Oz axis, $\lambda_\parallel/4$ apart, associated with opposite circular polarizations of the light. This accounts for the antiferromagnetic order of this 2D optical lattice, generalizing the order of the initial 1D configuration.

To evaluate the characteristics of the atomic motion near the bottom of a potential well, we use the harmonic approximation. This model is satisfactory for the lowest bound levels and should give a reasonable estimate of the atomic vibrational frequencies. Without loss of generality, we consider a lattice site at which the light polarization is purely σ^-. In the vicinity of this location, the in-

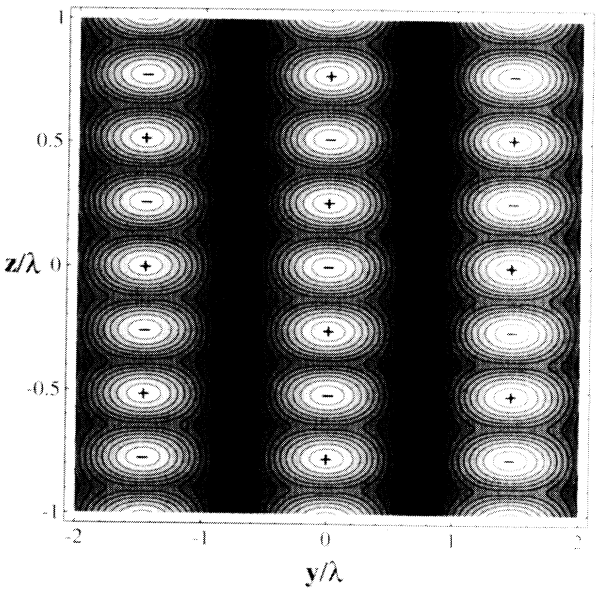

FIG. 5. Topography of the optical potential for the case of the 2D generalization of the lin⊥lin configuration presented in Sec. III A. The minima of the optical potential (associated with larger light shifts) are represented by the lightest zones of the figure. The sign of the circular polarization inside the potential wells is given. Atoms are expected to be localized inside the potential wells, which are regularly distributed on a lattice of the type presented in Fig. 2(a). Darker zones correspond to local maxima of the optical potential.

tensities of the circularly polarized field components are given by

$$\frac{I_+(\mathbf{r})}{I_0} \approx K_{\parallel}^2 z^2 , \tag{20a}$$

$$\frac{I_-(\mathbf{r})}{I_0} \approx 1-\frac{1}{2}K_{\perp}^2 y^2 - K_{\parallel}^2 z^2 , \tag{20b}$$

$$\frac{I_z(\mathbf{r})}{I_0} \approx \frac{\tan^2\vartheta}{2} K_{\perp}^2 y^2 , \tag{20c}$$

where $I_0=2E_0^2$. These expressions allow the evaluation of the harmonic approximation to the optical potential about a chosen minimum:

$$V_{\rm opt}^{(-)}(\mathbf{r}) \approx \frac{3U_0}{8I_0}[I_-(\mathbf{r})+I_z(\mathbf{r})+I_+(\mathbf{r})/3] , \tag{21}$$

where $|U_0|$ is the depth of the 1D potential wells ($U_0 \approx -\frac{4}{3}D^2E_0^2/\hbar\Delta$) [8,10]. One notices in Eq. (21) that the potential is not proportional simply to the sum of the intensities of the circular components (weighted by the appropriate Clebsch-Gordan coefficients of the $J_g=\frac{1}{2}\rightarrow J_e=\frac{3}{2}$ transition), as was the case in 1D, but that the π component of the light also makes an important contribution due to Zeeman coherences between the two ground-state sublevels. From Eqs. (20) and (21), we deduce expressions for the vibrational frequencies inside the 2D potential wells:

$$\Omega_y = \frac{|U_0|}{2\hbar}\left[\frac{3E_{R\perp}}{|U_0|}(1-\tan^2\vartheta)\right]^{1/2} ,$$
$$\Omega_z = \frac{|U_0|}{\hbar}\left[\frac{E_{R\parallel}}{|U_0|}\right]^{1/2} , \tag{22}$$

where $E_{R\parallel}=\hbar^2K_{\parallel}^2/2M$ and $E_{R\perp}=\hbar^2K_{\perp}^2/2M$ are quantities proportional to the recoil energy (M is the atomic mass). Note that Ω_y vanishes for $\vartheta=\vartheta_c=45°$, showing a modification of the topography of the potential. For $\vartheta>\vartheta_c$, the atoms are no longer expected to be localized in potential wells corresponding to a purely circular light polarization. Because of the importance of the π component of the incident light, new minima of the optical potential appear at points where the light polarization is almost linear and parallel to Oz. It should be noted, however, that there are other choices for the field amplitudes in this polarization configuration which permit us to have circularly polarized light at the potential minima (but with respect to a different axis) when $\vartheta>\vartheta_c$ [21].

B. Examples of 3D lattices

1. *Fields polarized along the Ox and Oy directions*

We first consider splittings performed along the lines of Sec. II C 3. The y-polarized beam of the lin⊥lin configuration is split into two beams propagating in the xOz plane and making an angle $2\theta_x$, while the x-polarized beam is split into two beams making an angle $2\theta_y$ and propagating in the yOz plane [see Fig. 1(e)]. The Oz axis is the bisector of the propagation directions of the x- and y-polarized beams. The four incident wave vectors are given by Eqs. (12), where $\mathbf{k}_1,\mathbf{k}_2$ are associated with the y-polarized beam and $\mathbf{k}_3,\mathbf{k}_4$ are the wave vectors of the x-polarized beams.

We call the common amplitude of the four incident traveling waves E_0. The circular components of the field are respectively equal to

$$E_{\pm}(\mathbf{r}) = \sqrt{2}E_0 e^{iK_-z}[\cos(K_x x)e^{iK_+z} \mp \cos(K_y y)e^{-iK_+z}] , \tag{23a}$$

$$E_z(\mathbf{r}) = 0 . \tag{23b}$$

In the case of the $J_g=\frac{1}{2}\rightarrow J_e=\frac{3}{2}$ atomic transition, the light-shift operator is diagonal in the basis of the ground-state magnetic sublevels, as in the initial 1D case [8]. Therefore, the expression of the optical bipotential $V_{\mp}$, depending on the ground-state sublevel, can be given as a function of the intensities of the circular components of the field

$$V_{\pm}(\mathbf{r}) = I_{\pm} + \tfrac{1}{3}I_{\mp} . \tag{24}$$

Two sections of $V_{\rm opt}(x,y,z)$ ($V_{\rm opt}$ is the minimum of $V_{\mp}$) have been plotted in Figs. 6(a) and 6(b). The first one is in the xOy plane and the second is in the xOz plane. The optical potential minima correspond to the white zones of the figure and are located at

$$\mathbf{R}_{l,m,n} = l\frac{\lambda_x}{2}\mathbf{e}_x + m\frac{\lambda_y}{2}\mathbf{e}_y + n\frac{\lambda_+}{4}\mathbf{e}_z \quad (l,m,n \text{ integers}) . \tag{25}$$

Two kinds of sites, with regard to the light polarization, are distinguished: $\mathbf{R}_{l,m,n}^{(-)}$ with $l+m+n$ even, where the light is σ^- circularly polarized [see, for instance, Eqs. (23a) and (23b)], and $\mathbf{R}_{l,m,n}^{(+)}$ with $l+m+n$ odd, which corresponds to σ^+-polarized light. This field configuration is thus appropriate for an optical lattice, whatever the values of θ_x and θ_y. The lattice structure for this field configuration has been discussed in Sec. II C 3. The basis of the lattice consists of two adjacent potential minima, $\lambda_+/4$ apart along Oz, and corresponding to opposite circular polarizations of the light (see Fig. 4). The lattice therefore has an antiferromagnetic structure. The dimension of the primitive cell is of course changed when the angles θ_x and θ_y are modified.

The persistent relationship to the initial 1D configuration is obvious when the 3D potential is viewed along a line parallel to Oz such as $x=y=0$. Apart from the distance between two minima, which is $\lambda_+/4$ instead of $\lambda/4$, one finds exactly the same optical potential as in the 1D case. However, the behavior of atoms in these 3D lattices is more complex than in the 1D case. While an atom following the $x=y=0$ line will experience an efficient Sisyphus cooling, this is not the case for an atom following one of the lines where the light keeps the same circular polarization [these lines are solutions of $E_+(\mathbf{r})=0$ or $E_-(\mathbf{r})=0$, where $E_{\pm}$ is given by Eq. (23a)]. One can also note the occurrence of lines parallel to Oz

where the light intensity vanishes and where the optical potential is a maximum. These lines correspond to the darkest zones of Fig. 6. Except for the replacement of λ_x and λ_y by λ, the potential in the xOy plane [Fig. 7(a)] is very much like the potential of the 2D lattice studied experimentally by Hemmerich and Hänsch [11] and theoretically by Berg-Sørensen *et al.* [22].

We now turn to the characteristics of the motion of an atom bound in one of these potential wells. Again, without loss of generality, we consider a lattice site at which the light polarization is purely σ^-. The intensities

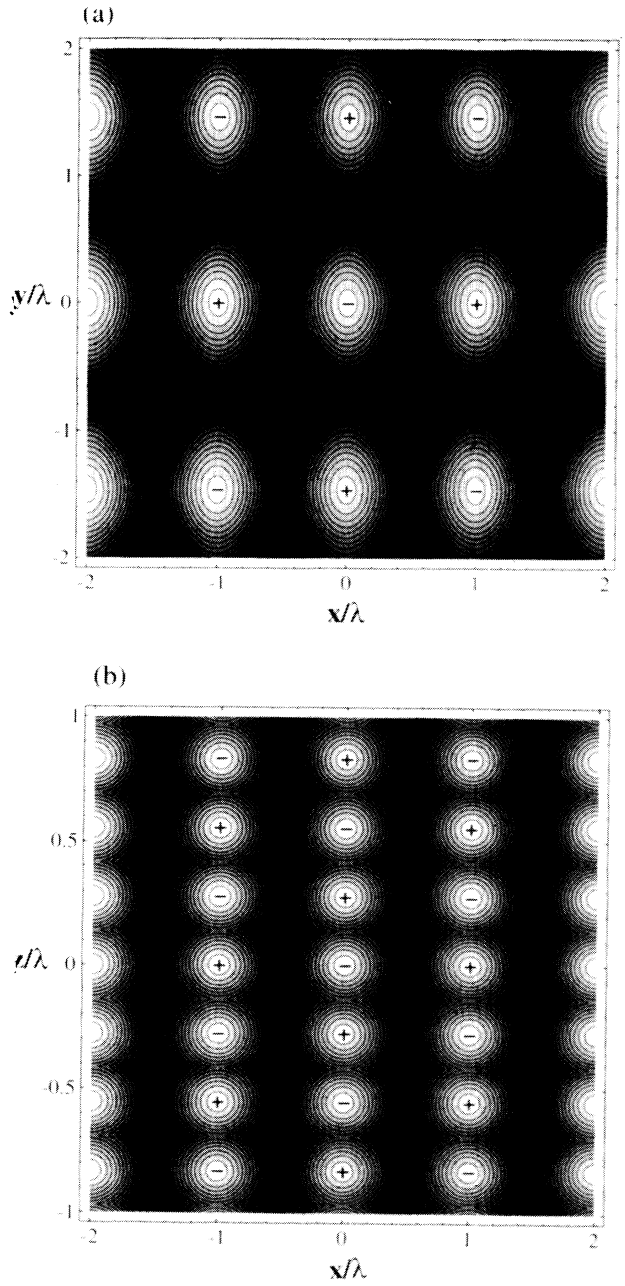

FIG. 6. Optical potential map for the 3D configuration of Sec. III B 1 in the particular case where $\theta_x = 20°$ and $\theta_y = 30°$. The different gray levels correspond to different values of the light shifts, the white zones denoting the potential minima. (a) Section of the potential in the xOy plane ($z = 0$). The projection of the lattice in this plane is very similar to the 2D lattice obtained using two mutually orthogonal standing waves of Refs. [11,22]. Totally dark zones are present, indicating destructive interference between the four cooling beams. (b) Section in the xOz plane ($y = 0$). In this plane, the form of the initial 1D configuration persists along some lines parallel to Oz.

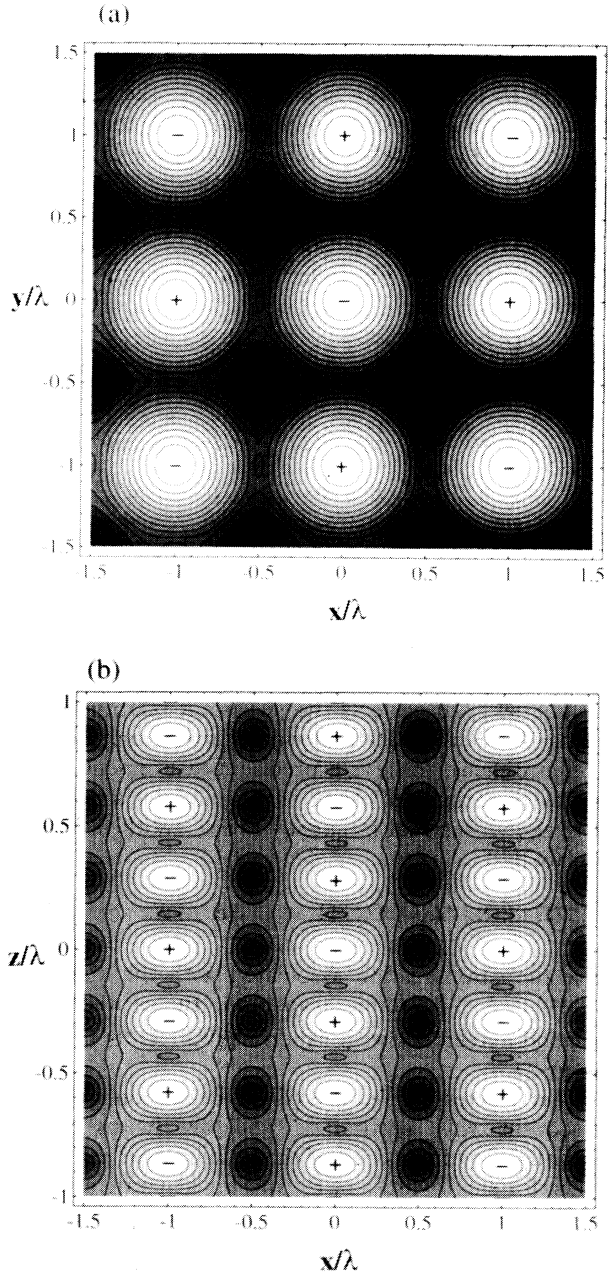

FIG. 7. Optical potential map for the 3D configuration of Sec. III B 2 in the particular case where $\theta_x = \theta_y = 30°$. The different gray levels correspond to different values of the light shifts, the white zones denoting the potential minima. The topography is very similar to the one of Fig. 6 because the two configurations originate from the same 1D situation. Important differences, however, exist due to the presence of π polarized light in the present scheme. (a) Section of the potential in the xOy plane ($z = 0$). Totally dark zones are now absent because of the π polarized light. (b) Section in the xOz plane ($y = 0$).

of the circularly polarized field components are, in the harmonic approximation,

$$\frac{I_+(\mathbf{r})}{I_0} \approx 4K_+^2 z^2 , \tag{26a}$$

$$\frac{I_-(\mathbf{r})}{I_0} \approx 4-2K_x^2 x^2-2K_y^2 y^2-4K_+^2 z^2 , \tag{26b}$$

$$I_z(\mathbf{r})=0 , \tag{26c}$$

where $I_0=2E_0^2$. It should be noted that in the harmonic approximation I_+ depends only on z. This means that the probability of optical pumping towards the other Zeeman sublevel is not expected to vary rapidly with the vibrational quantum numbers v_x and v_y for small values of v_x and v_y. The optical potential given by (24) leads to the following expressions for the harmonic vibrational frequencies:

$$\Omega_x=\frac{|U_0|}{\hbar}\left[\frac{3E_{Rx}}{|U_0|}\right]^{1/2},$$

$$\Omega_y=\frac{|U_0|}{\hbar}\left[\frac{3E_{Ry}}{|U_0|}\right]^{1/2}, \tag{27}$$

$$\Omega_z=2\frac{|U_0|}{\hbar}\left[\frac{E_{R+}}{|U_0|}\right]^{1/2},$$

where $E_{Rx}=\hbar^2K_x^2/2M$, $E_{Ry}=\hbar^2K_y^2/2M$, and $E_{R+}=\hbar^2K_+^2/2M$. The fact that the vibration frequency along the Oz axis is given by an expression similar to that of the 1D case [10] reflects the persistent relationship to the initial 1D configuration along this direction. Because it is often difficult to have a precise measurement of E_0, the easiest experimental check of this model is a measurement of the vibrational frequency ratios. With the above values, we find

$$\Omega_y/\Omega_x=K_y/K_x, \quad \Omega_z/\Omega_x=\frac{2}{\sqrt{3}}K_+/K_x . \tag{28}$$

Despite the simplification associated with the choice of the $J_g=\frac{1}{2}\rightarrow J_e=\frac{3}{2}$ atomic transition, these predictions are in good agreement with experimental results for cesium atoms [15].

Another interesting feature of the beam configuration discussed in this section is the ability to adjust significantly the dimensions of the lattice's unit cell. One can thus, for small values of θ_x and θ_y, generate a lattice where the nearest-neighbor site is at a distance of the order of several optical wavelengths. A simple method for obtaining large separations along the z axis is to reverse the wave vectors of both x-polarized beams of Fig. 1(e). It turns out then that the only difference with the previous discussion is that K_+ is replaced by K_- [see Eq. (13)] in the above calculations. This situation is rather surprising from the point of view of its one-dimensional analog. In the 1D limit ($\theta_x\rightarrow\pi,\theta_y\rightarrow 0$), one gets two linearly cross polarized copropagating traveling waves, i.e., a single traveling wave with a fixed elliptic polarization. In such a case, there is no polarization gradient of the field and the only force acting on the atomic system is the radiation pressure, which pushes the atoms along the z direction. The 3D situation is quite different. Although there is still a radiation pressure which induces a net force along Oz, the reactive force associated with the light shifts should be dominant whenever $K_+|\Delta|/k\Gamma\gg 1$ [23]. This *reversed tetrahedral* beam configuration can lead, with a convenient choice of angles, to optical lattices with a unit cell volume of the order of $600\lambda^3$ (where λ is the common wavelength of the four cooling beams). For instance, if one chooses $\theta_x\approx 160°$ and $\theta_y\approx 5°$, the spacings between neighboring sites in the unit cell are $\Delta x=\lambda_x\approx 3\lambda$, $\Delta y=\lambda_y\approx 11\lambda$, and $\Delta z=\lambda_+/2\approx 18\lambda$. This kind of *macroscopic* optical lattice might directly be observed experimentally, provided that the cooling process is efficient enough to produce the required atomic localization [24].

2. *Fields linearly polarized in the xOz and yOz planes*

We now discuss another way to generalize the 1D lin⊥lin scheme. The initial two beams of Fig. 1 are split into four beams by the method described in Sec. III C 3 [see Fig. 1(e)], but the beams propagating in the xOz plane are now linearly polarized in the xOz plane and the beams propagating in the yOz plane are linearly polarized in the yOz plane. The amplitudes of the four fields are chosen such that $\mathcal{E}_{xz}=E_0/\cos\theta_x$ and $\mathcal{E}_{yz}=E_0/\cos\theta_y$, where $\mathcal{E}_{xz}$ ($\mathcal{E}_{yz}$) is the electric-field amplitude of the beams propagating in the xOz (yOz) plane. The expressions of the circularly polarized components of the electric field are equal to

$$E_\pm(\mathbf{r})=\sqrt{2}E_0 e^{iK_-z}[\pm\cos(K_x x)e^{iK_+z} - \cos(K_y y)e^{-iK_+z}] , \tag{29a}$$

$$E_z(\mathbf{r})=2E_0 e^{iK_-z}[\tan\theta_y \sin(K_y y)e^{-iK_+z} + i\tan\theta_x \sin(K_x x)e^{iK_+z}] . \tag{29b}$$

As seen in Sec. II, the form of the Bravais lattice is determined by the geometry of the propagation directions of the cooling beams, so that the lattice is the same as in Sec. III B 1 (also see Fig. 4). Despite this similarity between the two configurations, several differences arise from the fact that the total electric field's component along the Oz axis is now generally different from zero. The presence of π-polarized light, which was absent in the 1D case as well as in the preceding 3D generalization, has several consequences. A first consequence is that the light-shift operator is no longer diagonal in the basis of the ground-state Zeeman sublevels. Indeed, coherences between the $|g,+\frac{1}{2}\rangle$ and the $|g,-\frac{1}{2}\rangle$ magnetic levels are found (as in the 2D configuration considered in Sec. III A). A second consequence is that the wires found in Fig. 7, where the light intensity is zero, do not exist in the present situation.

By diagonalizing the light-shift operator, we get the expression for the optical potential. Sections of V_{opt} in the xOy and xOz planes are shown in the Figs. 7(a) and 7(b) for the case where $\theta_x=\theta_y=30°$. We notice in these figures the absence of totally dark zones associated with

zero light intensity, as mentioned above. The darkest zones in the figures correspond to the maxima of the potential and are associated with points where the light polarization is purely linear along the *Oz* direction. The locations of the potential minima are still given by Eqs. (25) and correspond to points where the light is purely circular (alternatively σ^+ and σ^- polarized). From the expressions (28a) and (28b), one can observe that increasing the angles between the cooling beams results in an increase of the π-polarized light intensity, while the amount of $\sigma^{\pm}$ circularly polarized light remains constant (this is because of the particular choice of normalization for the field amplitudes). Thus increasing the angles leads to shallower potential wells. In fact, we will show that beyond a certain angle the topography of the optical potential exhibits a dramatic change because the deepest minima are then located in areas where the light polarization is linear.

In order to discuss the nature of the potential minima and to find the atomic vibrational frequencies, we develop the expressions of the light intensities in the vicinity of a σ^--polarized site of the potential

$$\frac{I_+(\mathbf{r})}{I_0}\approx 4K_+^2 z^2 , \tag{30a}$$

$$\frac{I_-(\mathbf{r})}{I_0}\approx 4-2K_x^2x^2-2K_y^2y^2-4K_+^2z^2 , \tag{30b}$$

$$\frac{I_z(\mathbf{r})}{I_0}\approx 2[K_x^2x^2\tan^2\theta_x+K_y^2y^2\tan^2\theta_y] . \tag{30c}$$

The optical potential in the vicinity of such a site can be expressed as a function of the intensities [see Eq. (21)]. In this approximation, one obtains the following vibrational angular frequencies:

$$\Omega_x=\frac{|U_0|}{\hbar}\left[3(1-\tan^2\theta_x)\frac{E_{Rx}}{|U_0|}\right]^{1/2},$$

$$\Omega_y=\frac{|U_0|}{\hbar}\left[3(1-\tan^2\theta_y)\frac{E_{Ry}}{|U_0|}\right]^{1/2}, \tag{31}$$

$$\Omega_z=2\frac{|U_0|}{\hbar}\left[\frac{E_{R+}}{|U_0|}\right]^{1/2}.$$

The frequency Ω_x vanishes for $\theta_x=45°$. As in the 2D case (see Sec. II A), the critical value $\theta_c=45°$ is associated with a modification of the topography of the optical potential. When θ_x or θ_y reaches this value, the potential undergoes a *saddle node bifurcation* and the relevant harmonic term in the development of $V_{\rm opt}(x,y,z)$ vanishes. The form of the potential wells is then drastically altered (see Fig. 8). In fact, beyond this critical angle, the deepest potential minima are no longer located at points where the light is purely circular and thus the properties of the lattice should be considerable modified. The topography of the optical potential beyond the bifurcation point is illustrated by Figs. 9(a) and 9(b) in the particular case when $\theta_x=\theta_y=60°$. One notices that the deepest minima are now located at

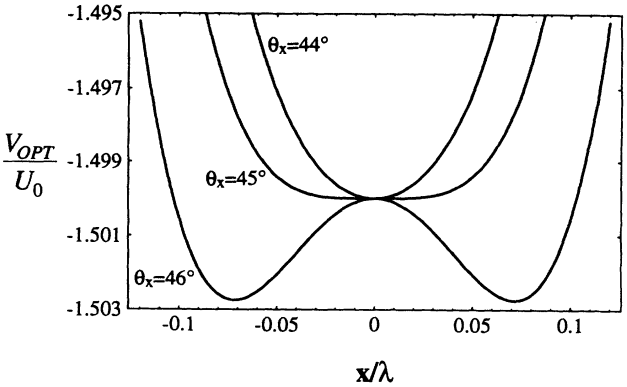

FIG. 8. Curve showing the variations of the optical potential versus x along $y=z=0$ and for several values of θ_x (configuration of Sec. III B 2). The potential undergoes a saddle node bifurcation for $\theta_x=45°$, implying a profound modification of the topography presented in Fig. 7. This transition is essentially related to the presence of π-polarized light in this configuration, inducing Zeeman coherences between the ground-state magnetic sublevels.

$$\mathbf{R}^{(\pi)}_{l,m,n}=(2l+1)\frac{\lambda_x}{4}\mathbf{e}_x+(2m+1)\frac{\lambda_y}{4}\mathbf{e}_y+(2n+1)\frac{\lambda_+}{8}\mathbf{e}_z$$

(l,m,n integers) , (32)

where the total electric field is aligned along the *Oz* direction, as expected from the discussion above.

3. *Umbrellalike configuration*

As mentioned in Sec. II C 2, a different way of splitting the 1D lin⊥lin configuration can be obtained by splitting one of the initial beams (for example, the y-polarized beam) into three beams, the counterpropagating beam (x polarized) being unchanged. The three beams obtained after splitting have linear polarizations in the yOz plane. This *umbrellalike* geometry is illustrated in Fig. 1(c) [see also Eq. (9)]. To obtain a purely circular polarization at the bottoms of the potential wells, we make the following choice for the amplitudes: the x-polarized wave (associated with $\mathbf{k}_3$) has an amplitude $\mathcal{E}_3=E_0$, whereas the three other beams (associated with $\mathbf{k}_0,\mathbf{k}_1,\mathbf{k}_2$) have electric-field amplitudes given by $\mathcal{E}_0=E_0/3$ and $\mathcal{E}_1=\mathcal{E}_2=E_0\sqrt{3+\cos^2\vartheta}/6\cos\vartheta$, respectively. Note that the choice of polarization breaks the rotation symmetry around *Oz*. We now write the circularly polarized components of the total electric field

$$E_{\pm}(\mathbf{r})=\frac{1}{\sqrt{2}}E_0e^{-ikz}\left[\mp 1+\tfrac{1}{3}e^{i(2K_{\parallel}z-K_{\perp}x)}+\tfrac{2}{3}\cos\left[\frac{\sqrt{3}K_{\perp}y}{2}\right]e^{i(2K_{\parallel}z+K_{\perp}x/2)}\right], \tag{33a}$$

$$E_z(\mathbf{r})=\frac{1}{\sqrt{3}}E_0\tan\vartheta\sin\left[\frac{\sqrt{3}K_{\perp}y}{2}\right]e^{-i(kz+K_{\perp}x/2)} . \tag{33b}$$

We carry out the calculation of the optical potential by

diagonalizing the light-shift operator in the ground-state Zeeman sublevel basis. Sections of the potential in the xOy and xOz planes are respectively shown in Figs. 10(a) and 10(b) for the case of $\vartheta = 30°$. The potential minima, represented by the white zones, correspond alternatively to σ^+ and σ^- light polarization with respect to the Oz axis. More explicitly, σ^--polarized sites are located at

$$\mathbf{R}^{(-)}_{l,m,n} = l\frac{\lambda_\perp}{3}\mathbf{e}_x + (2m+l)\frac{\lambda_\perp}{\sqrt{3}}\mathbf{e}_y + (3n+l)\frac{\lambda_\parallel}{6}\mathbf{e}_z$$

(l,m,n integers) . (34a)

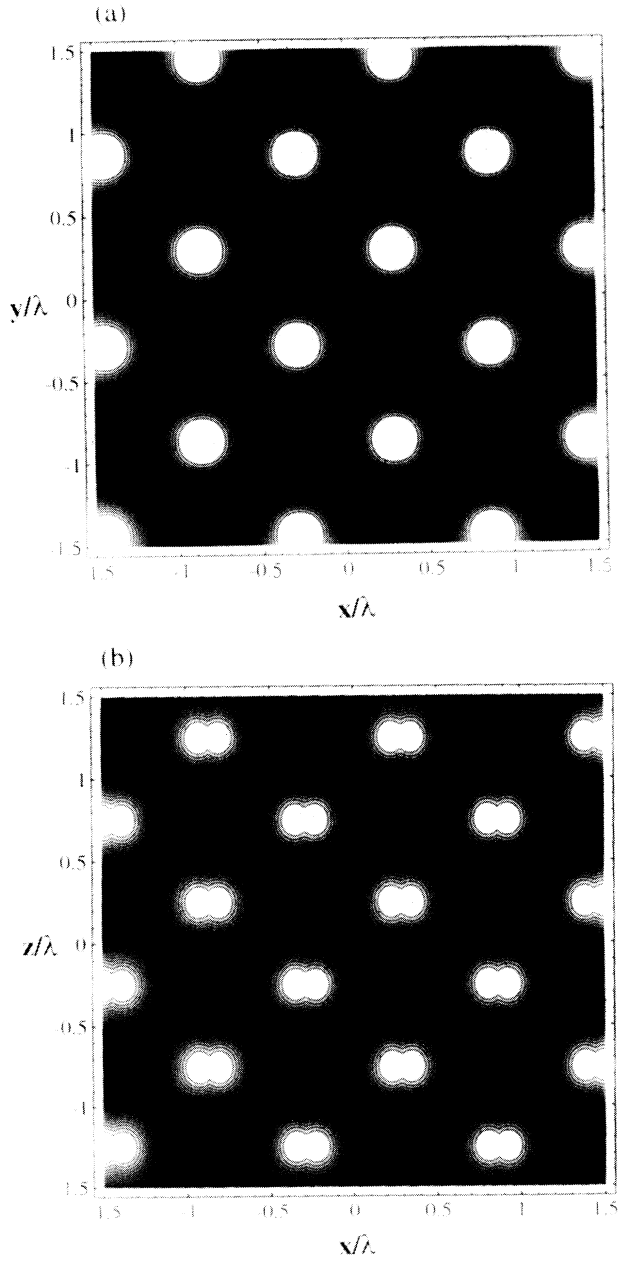

FIG. 9. Potential map for the configuration studied in Sec. III B 2, for $\theta_x = \theta_y = 60°$ (i.e., beyond the critical angle). The minima of the optical potential are now located in regions corresponding to π polarization of the light. (a) Section in the x-y plane ($z = \lambda_+/8$). (b) Section in the x-z plane ($y = \lambda_y/4$).

Positions of the minima associated with σ^+ polarization of light are given by

$$\mathbf{R}^{(+)}_{l,m,n} = l\frac{\lambda_\perp}{3}\mathbf{e}_x + (2m+l)\frac{\lambda_\perp}{\sqrt{3}}\mathbf{e}_y + (3n+l+\tfrac{3}{2})\frac{\lambda_\parallel}{6}\mathbf{e}_z$$

(l,m,n integers) . (34b)

The basis of the optical lattice consists of two adjacent potential wells along the z axis, associated with orthogonal circular polarizations. The distance between the two

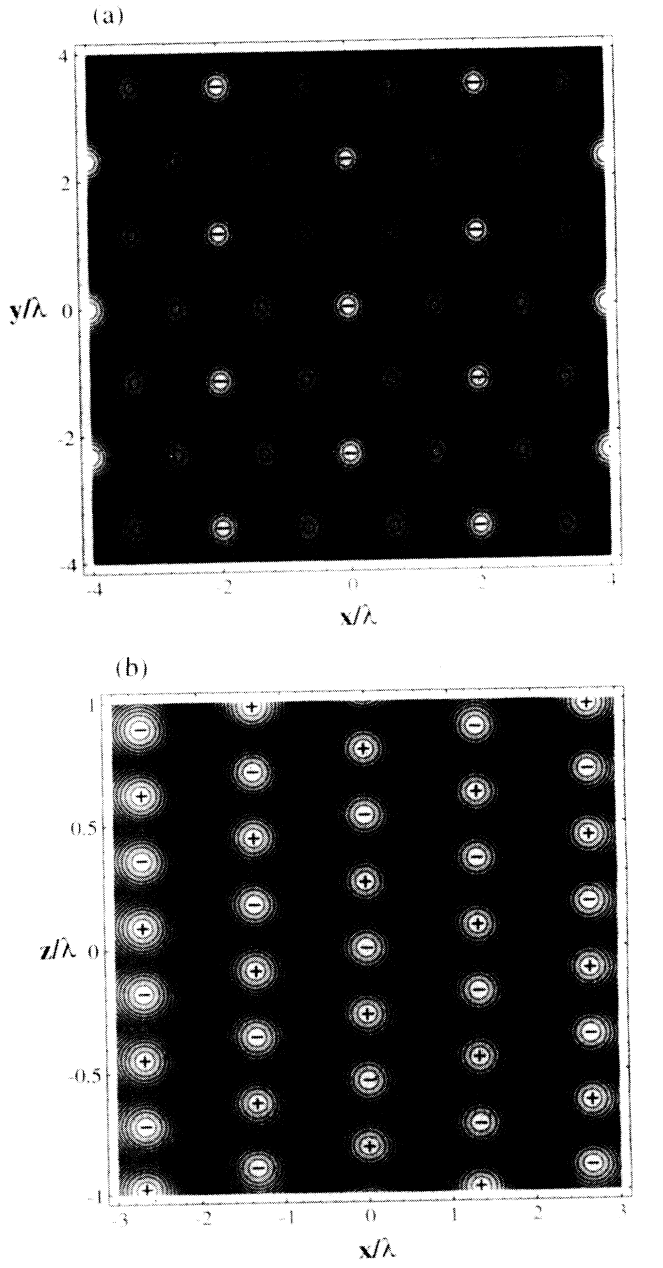

FIG. 10. Topography of the optical potential for the umbrellalike configuration discussed in Sec. III B 3. (a) Section in the plane $z = 0$. The potential minima are on a 2D hexagonal lattice. (b) Section of the potential in the plane $y = 0$. Here too the relationship to the initial 1D configuration persists along lines parallel to Oz. The form of the 3D optical lattice is shown in Fig. 3.

minima is $\lambda_{\parallel}/4$. Here again, one gets an antiferromagnetic order.

We now estimate the vibrational frequencies near the bottoms of the potential wells by using the harmonic approximation. In the vicinity of a σ^--polarized site, the expressions for the intensities of the circular components of the field are

$$\frac{I_+(\mathbf{r})}{I_0}\approx K_{\parallel}^2 z^2 , \tag{35a}$$

$$\frac{I_-(\mathbf{r})}{I_0}\approx 1-\frac{1}{4}K_{\perp}^2 x^2-\frac{1}{4}K_{\perp}^2 y^2-K_{\parallel}^2 z^2 , \tag{35b}$$

$$\frac{I_z(\mathbf{r})}{I_0}\approx \frac{\tan^2\vartheta}{8}K_{\perp}^2 y^2 . \tag{35c}$$

Using Eq. (21) for the potential, one obtains the following expressions for the vibrational frequencies:

$$\Omega_x=\frac{|U_0|}{\hbar}\left[\frac{3E_{R\perp}}{8|U_0|}\right]^{1/2},$$

$$\Omega_y=\frac{|U_0|}{\hbar}\left[\frac{3}{8}\left[1-\frac{\tan^2\vartheta}{2}\right]\frac{E_{R\perp}}{|U_0|}\right]^{1/2}, \tag{36}$$

$$\Omega_z=\frac{|U_0|}{\hbar}\left[\frac{E_{R\parallel}}{2|U_0|}\right]^{1/2}.$$

The value $\vartheta_c=\arctan(\sqrt{2})\approx 54.7°$ appears as a critical value of the angle for which the vibration frequency along the y axis vanishes. This value is associated with a modification of the potential wells along the y direction, leading to a different topography of the optical potential. It can be noted that no critical value of ϑ is found in the expression for Ω_x. This is a consequence of the beam configuration not being symmetric in x and y.

IV. GENERALIZATION OF THE MASE CONFIGURATION

This section is devoted to the presentation of a possible three-dimensional extension of the 1D MASE configuration [6,7,9]. The 1D scheme consists of two traveling waves of common frequency ω_L, having the same circular polarization and opposite propagation directions along the Oz axis, and a weak transverse static magnetic field applied along the Ox axis. In this situation, the local polarization is uniformly circular. The role of the magnetic field is to mix the ground-state sublevels in the vicinity of the nodes of the electric field. Cooling arises from the combined effect of optical pumping and Larmor precession of the ground states.

In order to extend the 1D situation to three dimensions, we use the four beam geometry of Sec. II C 3. The polarizations of the four beams of Fig. 1(e) are now elliptical and respectively given by

$$\mathbf{u}_1=\frac{1}{\sqrt{2+\tan^2\theta_x}}[-\mathbf{e}_x+i\mathbf{e}_y+\tan(\theta_x)\mathbf{e}_z] , \tag{37a}$$

$$\mathbf{u}_2=\frac{1}{\sqrt{2+\tan^2\theta_x}}[-\mathbf{e}_x+i\mathbf{e}_y-\tan(\theta_x)\mathbf{e}_z] , \tag{37b}$$

$$\mathbf{u}_3=\frac{1}{\sqrt{2+\tan^2\theta_y}}[-\mathbf{e}_x+i\mathbf{e}_y+i\tan(\theta_y)\mathbf{e}_z] , \tag{37c}$$

$$\mathbf{u}_4=\frac{1}{\sqrt{2+\tan^2\theta_y}}[-\mathbf{e}_x+i\mathbf{e}_y-i\tan(\theta_y)\mathbf{e}_z] . \tag{37d}$$

The elliptic polarizations of the incident waves are thus chosen such that the projection of each field onto the xOy plane is σ^+ circularly polarized. The two traveling waves propagating in the xOz plane have amplitudes $\mathcal{E}_{xz}=E_0\sqrt{1+\cos^2\theta_x}/\cos\theta_x$, whereas the electric-field amplitudes of the waves that propagate in the yOz plane are given by $\mathcal{E}_{yz}=E_0\sqrt{1+\cos^2\theta_y}/\cos\theta_y$. With this convention, the circular components of the laser field are

$$E_+(\mathbf{r})=\sqrt{2}E_0 e^{iK_-z}[\cos(K_x x)e^{iK_+z}+\cos(K_y y)e^{-iK_+z}] , \tag{38a}$$

$$E_-(\mathbf{r})=0 , \tag{38b}$$

$$E_z(\mathbf{r})=E_0 e^{iK_-z}[\tan\theta_y\sin(K_y y)e^{-iK_+z}-i\tan\theta_x\sin(K_x x)e^{iK_+z}] , \tag{38c}$$

where K_x, K_y, and $K_\pm$ are given by Eq. (13). Compared to the situations presented in Secs. III B 1 and III B 2 the spatial periodicity of the field is the same, but the basis of the lattice is different because in the present case the light has no σ^- component.

We calculate the eigenvalues and the eigenfunctions of the effective Hamiltonian (light-shift operator) to evaluate the optical potential. In Figs. 11(a) and 11(b), sections of V_{opt} are shown respectively in the xOy and the xOz planes. The potential minima are located at

$$\mathbf{R}^{(+)}_{l,m,n}=l\frac{\lambda_x}{2}\mathbf{e}_x+m\frac{\lambda_y}{2}\mathbf{e}_y+n\frac{\lambda_+}{4}\mathbf{e}_z$$

$$(l+m+n \text{ even}; \ l,m,n \text{ integers}) . \tag{39}$$

At these sites, the light is purely σ^+ polarized, as shown by Eqs. (38), and therefore the optical lattice is *ferromagnetic*. One also notices the occurrence of very dark zones in the figures, appearing near points where the total light intensity is zero. These are nodes of the laser field, associated with degenerate energy levels of the effective Hamiltonian. As in the 1D case, an additional magnetic field might be necessary to induce couplings between the Zeeman sublevels at these points. However, because of the π component of the lattice light, the 3D situation differs from the 1D case and in particular the eigenstates are space dependent in the 3D case. Nonadiabatic transitions between these states are possible and might permit us to achieve cooling even without a magnetic field.

We now turn to the evaluation of the vibrational frequencies for atoms localized near the bottoms of the potential wells. In the vicinity of a potential minimum, the intensities of the circularly and linearly polarized components of the light are given by

$$\frac{I_+(\mathbf{r})}{I_0}\approx 4-2K_x^2x^2-2K_y^2y^2-2K_+^2z^2 , \tag{40a}$$

$$I_-(\mathbf{r})=0\ , \tag{40b}$$

$$\frac{I_z(\mathbf{r})}{I_0}\approx\tfrac{1}{2}[K_x^2x^2\tan^2\theta_x+K_y^2y^2\tan^2\theta_y]\ . \tag{40c}$$

The optical potential in the harmonic approximation is given by Eq. (21) and reduces here to $V_{\rm opt}(\mathbf{r})\propto I_+(\mathbf{r})+I_z(\mathbf{r})$. The resulting angular vibration frequencies are

$$\Omega_x=\frac{|U_0|}{\hbar}\left[3\left[1-\frac{\tan^2\theta_x}{4}\right]\frac{E_{Rx}}{|U_0|}\right]^{1/2},$$

$$\Omega_y=\frac{|U_0|}{\hbar}\left[3\left[1-\frac{\tan^2\theta_y}{4}\right]\frac{E_{Ry}}{|U_0|}\right]^{1/2}, \tag{41}$$

$$\Omega_z=2\frac{|U_0|}{\hbar}\left[\frac{3E_{R+}}{2|U_0|}\right]^{1/2}.$$

These expressions permit us to find the critical values of the angles θ_x and θ_y for which the optical potential exhibits a saddle node bifurcation similar to the ones mentioned in the previous sections. Once again, this transition is essentially related to the presence of π-polarized light of which the relative importance increases for increasing angles. The critical value of the angles is given by $\theta_c=\arctan(2)\approx 63.4°$. Note that localization of atoms on a body-centered-cubic lattice [occurring for $\theta_x=\theta_y=\arccos(1/\sqrt{3})\approx 54.7°$, as shown in Sec. II C 3] is still possible.

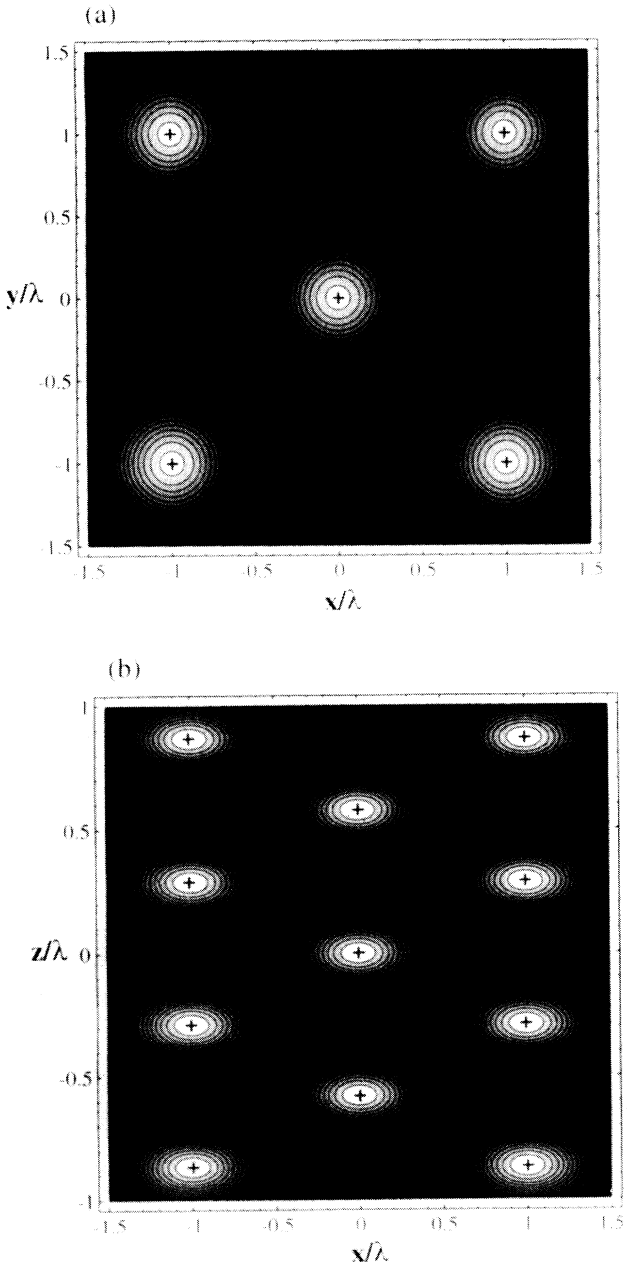

FIG. 11. Optical potential in the case of the 3D configuration proposed in Sec. IV for $\theta_x=\theta_y=30°$. The optical lattice has the same symmetry as the one considered in Sec. III B 1 (see Fig. 4), but the basis here consists of a single potential well (instead of two wells associated with opposite circular polarizations of light; see Fig. 4). The lattice is therefore ferromagnetic. Totally dark zones in the figure indicate regions where the light intensity is vanishing. (a) Section in the xOy plane ($z=0$). (b) Section in the xOz plane ($y=0$).

V. CONCLUSION

We have presented several field configurations that can lead to atomic localization at sites which are regularly distributed on a 2D or a 3D lattice and we have predicted some characteristics of the atomic motion inside such a potential well. Our study is a first step in the understanding of these optical lattices. The next step should be the study of the evolution of a single atom in such a lattice, to determine the probability of occupancy of the energy levels (i.e., the "*temperature*") and the long-range dynamics of the atom. It would also be interesting to consider several atoms and to take into account their mutual interactions (for example, through the field they radiate, such as in the experiment on *optical binding* performed with dielectric spheres [25]). One attractive problem is, for instance, to determine whether the atoms are always randomly distributed over the lattice or if some local or global order appears when the density increases. Another and totally different problem is the study of structures that are obtained with a greater than the minimum number of beams: because of the lack of spatial periodicity that is obtained in such a case, totally new features might be expected which are worthy of investigation.

APPENDIX: GENERALIZATION OF THE σ^+-σ^- CONFIGURATION

We present here a 3D generalization of the σ^+-σ^- cooling configuration [3,14]. The usual 1D situation involves two counterpropagating waves, with orthogonal circular polarizations, propagating along the Oz axis. In this case, the motion-induced atomic orientation of the ground state gives rise to unbalanced radiation pressures between the two beams, leading to a net friction force [3]. Although this field configuration does not give localization in the 1D case and is thus not expected to lead to an optical lattice in the 3D case, it seems interesting to study

the characteristics of the 3D extension to this cooling scheme. In particular, the rules given in Sec. II for the spatial periodicity should also be valid for these three-dimensional structures. The 3D configuration is illustrated using a $J_g=1\rightarrow J_e=2$ atomic transition. Potential maps are presented below allowing a study of the atomic motion in this 3D situation.

The 1D configuration is split according to the scheme of Sec. II C 3, so that the incident wave vectors are given by Eqs. (12). The four beams are elliptically polarized in a way such that the projections of the electric fields of the two beams propagating in the xOz (yOz) plane onto a plane orthogonal to the z axis have circular σ^+ (σ^-) polarizations:

$$\mathbf{u}_1=\frac{1}{\sqrt{2+\tan^2\theta}}[-\mathbf{e}_x+i\mathbf{e}_y+\tan(\theta)\mathbf{e}_z]\,, \tag{A1a}$$

$$\mathbf{u}_2=\frac{1}{\sqrt{2+\tan^2\theta}}[-\mathbf{e}_x+i\mathbf{e}_y-\tan(\theta)\mathbf{e}_z]\,, \tag{A1b}$$

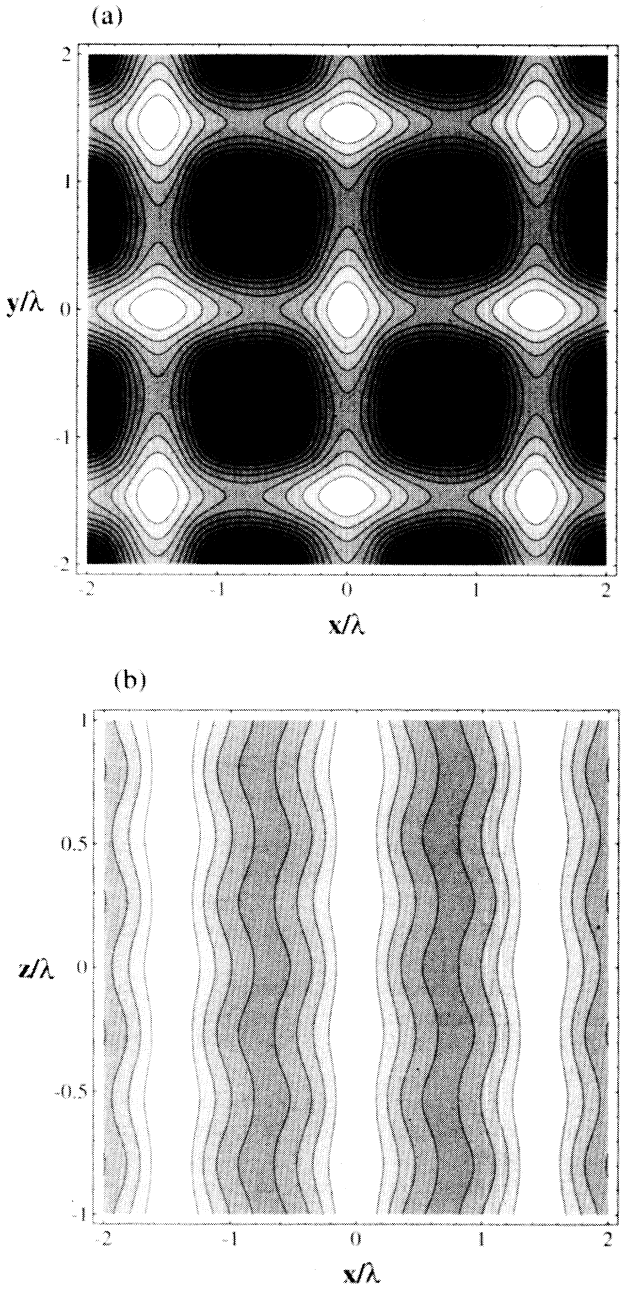

FIG. 12. Potential map for the generalization of the σ^+-σ^- configuration for $\theta_x=\theta_y=\theta=20°$. (a) Section in the plane $z=0$. The optical potential minima are located on a square lattice in this plane. The light polarization is linear at these sites. (b) Section in the plane $y=0$. *Wires* of minimum potential (white lines) are present. The light polarization forms a helix of pitch $\lambda_+/4$ as an atom moves along these lines.

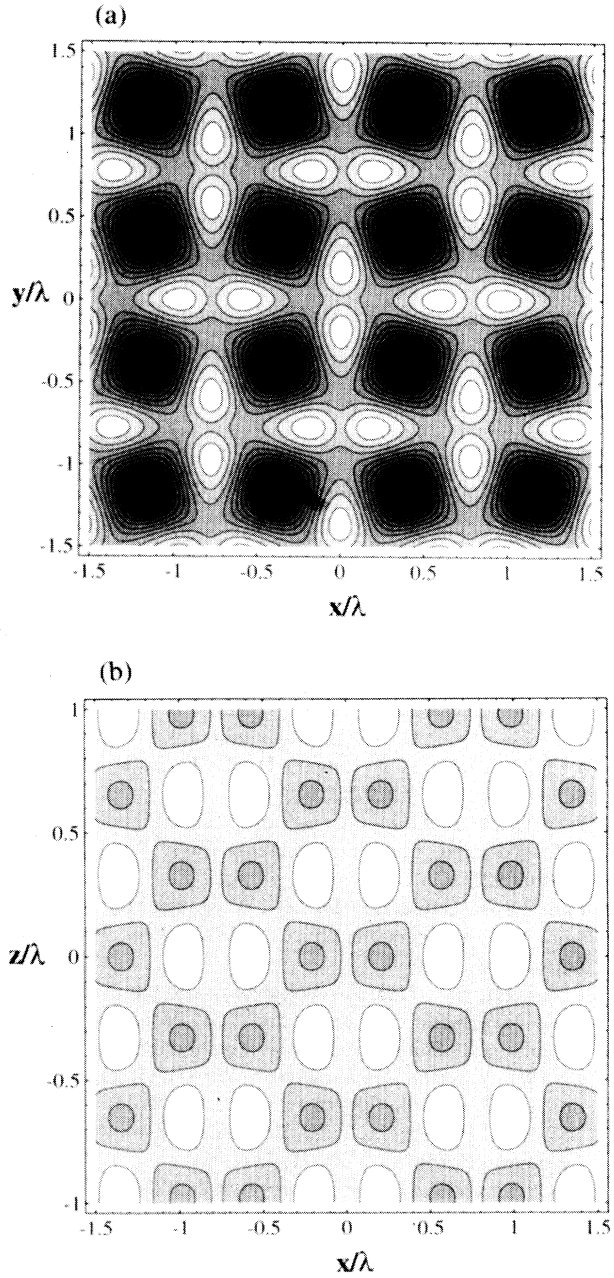

FIG. 13. Sections of the optical potential in the (a) xOy and (b) xOz planes for $\theta_x=\theta_y=\theta=40°$. As the angle θ has a value which is larger than the critical value, the topography of the potential is significantly modified. In particular, the wires of minimum potential along Oz disappear.

$$\mathbf{u}_3=\frac{1}{\sqrt{2+\tan^2\theta}}[\mathbf{e}_x+i\mathbf{e}_y+i\tan(\theta)\mathbf{e}_z]\ , \tag{A1c}$$

$$\mathbf{u}_4=\frac{1}{\sqrt{2+\tan^2\theta}}[\mathbf{e}_x+i\mathbf{e}_y-i\tan(\theta)\mathbf{e}_z]\ , \tag{A1d}$$

where $\theta=\theta_x=\theta_y$. The amplitudes of the fields are chosen to be $\mathcal{E}_{xz}=\mathcal{E}_{yz}=E_0\sqrt{1+\cos^2\theta}$. We express the total laser field in circular coordinates

$$E_+(\mathbf{r})=\sqrt{2}E_0\cos(Kx)e^{iK_+z}\ , \tag{A2a}$$

$$E_-(\mathbf{r})=\sqrt{2}E_0\cos(Ky)e^{-iK_+z}\ , \tag{A2b}$$

$$E_z(\mathbf{r})=-E_0\tan(\theta)[\sin(Ky)e^{-iK_+z}-i\sin(Kx)e^{iK_+z}]\ , \tag{A2c}$$

where $K=K_x=K_y$. The field generally has an elliptic polarization. However, one notices the existence of *wires* parallel to *Oz* where the form of the initial 1D configuration persists. Indeed, an atom following a linear trajectory given by

$$\mathbf{r}_{m,n}(t)=m\frac{\lambda_x}{2}\mathbf{e}_x+n\frac{\lambda_y}{2}\mathbf{e}_y+z(t)\mathbf{e}_z\quad(m,n\ \text{integers}) \tag{A3}$$

experiences the influence of a field

$$\mathbf{E}_{m,n}(z)=\sqrt{2}E_0[(-1)^m e^{iK_+z}\boldsymbol{\varepsilon}_+ +(-1)^n e^{-iK_+z}\boldsymbol{\varepsilon}_-]\ . \tag{A4}$$

This field has a constant amplitude and a linear polarization in the *xOy* plane which rotates around *Oz*, forming a helix of pitch $\lambda_+/4$ as the atom moves along *Oz*. Therefore, one gets a 1D-like situation that can lead to orientational cooling.

The diagonalization of the light-shift operator in the ground state leads to the expression of the optical potential. The resulting topography is illustrated in Figs. 12(a) and 12(b) by sections of $V_{\text{opt}}(\mathbf{r})$ in the *xOy* and the *xOz* planes, respectively, for $\theta_x=\theta_y=20°$. It can be seen in these figures that the potential minima (represented by the white zones) are situated along the lines given by Eq. (A3). Thus one gets a mixed situation where spatial modulation of light shifts occurs in the *xOy* plane, while wires of minimum potential are present along directions orthogonal to this plane [26]. This situation may provide 2D atomic localization on a square lattice in the *xOy* plane and, at the same time, orientational cooling along the *Oz* axis.

It can be shown, by calculating the vibrational frequencies in the 2D potential wells, that the critical value of the angle θ is $\theta_c=\arctan(\frac{1}{2})\approx 26.6°$. When $\theta>\theta_c$, the potential wells of the 2D lattice exhibit profound modifications, as shown in Figs. 13(a) and 13(b). As can be seen in these figures, lines along which the field presents a structure similar to the one of the 1D σ^+-σ^- scheme are no longer associated with minima of the optical potential. Hence the atoms are no longer expected to be localized along these lines.

[1] See, for instance, Phys. Today **46** (6), 17 (1993).

[2] C. Cohen-Tannoudji, Ann. Phys. (Paris) **7**, 423 (1962).

[3] J. Dalibard and C. Cohen-Tannoudji, J. Opt. Soc. Am. B **6**, 2023 (1989); P. J. Ungar, D. S. Weiss, E. Riis, and Steven Chu, *ibid.* **6**, 2058 (1989).

[4] P. Verkerk, B. Lounis, C. Salomon, C. Cohen-Tannoudji, J.-Y. Courtois, and G. Grynberg, Phys. Rev. Lett. **68**, 3861 (1992).

[5] P. S. Jessen, C. Gerz, P. D. Lett, W. D. Phillips, S. L. Rolston, R. J. C. Spreeuw, and C. I. Westbrook, Phys. Rev. Lett. **69**, 49 (1992).

[6] R. Gupta, S. Padua, T. Bergeman, and H. Metcalf, in *Laser Manipulation of Atoms and Ions,* Proceedings of the International School of Physics "Enrico Fermi," Course CXVIII, Varenna, 1991, edited by E. Arimondo, W. Phillips, and F. Strumia (North-Holland, Amsterdam, 1992).

[7] B. Lounis, P. Verkerk, J.-Y. Courtois, C. Salomon, and G. Grynberg, Europhys. Lett. **21**, 13 (1993).

[8] Y. Castin and J. Dalibard, Europhys. Lett. **14**, 761 (1991).

[9] B. Sheehy, S. Q. Shang, P. Van Der Straten, S. Hatamian, and H. Metcalf, Phys. Rev. Lett. **64**, 858 (1990); C. Valentin, M. C. Gagné, J. Yu, and P. Pillet, Europhys. Lett. **17**, 133 (1992).

[10] J.-Y. Courtois and G. Grynberg, Phys. Rev. A **46**, 7060 (1992).

[11] A. Hemmerich and T. W. Hänsch, Phys. Rev. Lett. **70**, 410 (1993).

[12] G. Grynberg, B. Lounis, P. Verkerk, J.-Y. Courtois, and C. Salomon, Phys. Rev. Lett. **70**, 2249 (1993).

[13] A. Hemmerich, C. Zimmermann, and T. W. Hänsch, Europhys. Lett. **22**, 89 (1994).

[14] B. Lounis, J.-Y. Courtois, P. Verkerk, C. Salomon, and G. Grynberg, Phys. Rev. Lett. **69**, 3029 (1992).

[15] P. Verkerk, D. R. Meacher, A. B. Coates, J.-Y. Courtois, B. Lounis, S. Guibal, C. Salomon, and G. Grynberg, Europhys. Lett. **26**, 171 (1994).

[16] N. W. Ashcroft and N. D. Mermin, *Solid State Physics* (HRW International Editions, New York, 1976); C. Kittel, *Introduction to Solid State Physics* (Wiley, New York, 1962).

[17] Note that a process involving two beams $\mathbf{k}_i$ and $\mathbf{k}_j$ induces a change of momentum $\hbar(\mathbf{k}_i-\mathbf{k}_j)$, which can always be written as $\hbar(\mathbf{k}_1-\mathbf{k}_j)-\hbar(\mathbf{k}_1-\mathbf{k}_i)$.

[18] A supermolasses corresponds to a molasses where the beams are not aligned. As shown by Chu *et al.* [S. Chu, M. G. Prentiss, A. E. Cable, and J. E. Bjorkholm, in *Laser Spectroscopy VIII,* edited by W. Person and S. Svanberg (Springer-Verlag, Berlin, 1987), p. 58], the diffusion of atoms in a supermolasses involved times much longer than in a usual molasses. This behavior may be related to the lack of spatial periodicity that occurs for this beam configuration. By contrast, in a 3D lattice (or in a molasses) one can find directions along which an atom may travel without crossing a potential well or experiencing a cooling force. It may be that these directions disappear when the potential wells appear to be more randomly dis-

tributed.

[19] The last case is not straightforward to see from Eqs. (14). To convince oneself, one should rather use another set of primitive translation vectors in reciprocal space [which is of course not independent of the one given by (14)]: $\mathbf{a}_1'^* = \mathbf{a}_1^* = \mathbf{k}_2 - \mathbf{k}_4 = -K_x\mathbf{e}_x + K_y\mathbf{e}_y + 2K_+\mathbf{e}_z$, $\mathbf{a}_2'^* = \mathbf{k}_2 - \mathbf{k}_1 = -2K_x\mathbf{e}_x$, and $\mathbf{a}_3'^* = -\mathbf{a}_3^* = \mathbf{k}_2 - \mathbf{k}_3 = -K_x\mathbf{e}_x - K_y\mathbf{e}_y + 2K_+\mathbf{e}_z$. For $\cos\theta_x = \cos\theta_y = 1/\sqrt{3}$, these vectors have equal lengths and make a 60° angle with each other. This is the primitive cell of a face-centered-cubic lattice. To obtain the principal axes of the conventional cubic cell, perform a $3\pi/4$ rotation of the coordinates system around the z axis.

[20] C. Cohen-Tannoudji, in *Fundamental Systems in Quantum Optics*, Proceedings of the Les Houches Summer School of Theoretical Physics, Les Houches, 1990, Session LIII, edited by J. Dalibard, J.-M. Raimond, and J. Zinn-Justin (Elsevier Science, Amsterdam, 1992), p. 1.

[21] We now choose the field amplitudes to be $\mathcal{E}_1 = E_0$ for the x-polarized wave and $\mathcal{E}_{2,3} = E_0/2\sin\vartheta$ for the waves polarized in the yOz plane. Circularly polarized light at the bottoms of the potential wells can be found with these amplitudes, even for $\vartheta_c < \vartheta < \pi/2 + \vartheta_c$, but the reference axis should now coincide with Oy. The minima located at $\mathbf{R}_{m,n} = (2m+1)(\lambda_\perp/4)\mathbf{e}_y + (2n+1)(\lambda_\parallel/8)\mathbf{e}_z$ (where m and n are integers) correspond to points where the light is circularly polarized (the polarization being alternatively σ_y^+ or σ_y^-).

[22] K. Berg-Sørensen, Y. Castin, K. Mølmer, and J. Dalibard, Europhys. Lett. **22**, 663 (1993).

[23] An order of magnitude estimate of the radiation pressure force is given by $|\mathcal{F}_{\text{rad}}| \approx \hbar k \gamma_p$, where the optical pumping rate γ_p can be expressed either as a function of the saturation parameter s_0 or as a function of the laser detuning and the resonant Rabi frequency Ω_R associated with each traveling wave $\gamma_p \approx \Gamma s_0 \approx \Gamma(\Omega_R/\Delta)^2$. In the *reversed tetrahedral* configuration discussed here, the average force is directed along the Oz axis unit vector. One might think of compensating its contribution by the gravitational force, which can have the opposite direction to the former ($\mathcal{F}_g = M\mathbf{g}$). It can be shown indeed that the two opposing forces have the same order of magnitude when $|\Omega_R/\Delta| \approx 10^{-2}$.

[24] It is not the aim of the paper to predict the temperature in these lattices. In fact, even in the 1D case, the calculation of the temperature requires a difficult and lengthy calculation [8] (see also Y. Castin, Ph.D. thesis, Université Pierre et Marie Curie, 1992). It is possible, however, to estimate the temperature in the semiclassical limit by following the approach of Dalibard and Cohen-Tannoudji [3]. In this limit, the temperature is proportional to the ratio of the momentum diffusion coefficient $\mathcal{D}_p$ to the momentum friction coefficient α. When the distance between the potential hills increases, the friction coefficient is expected to decrease because Sisyphus events become less frequent. There are two types of terms in the diffusion coefficient. The most important one in the 1D case (and for $|\Delta| \gg \Gamma$) is associated with the fluctuation of the cooling force (and corresponds to jumps between two potential curves). This term varies in the same way as the friction force when the distance between the hills varies. Thus, as long as this diffusion coefficient $\mathcal{D}_p''$ remains the dominant term, the temperature of the lattice does not change. However, there is another mechanism for diffusion associated with spontaneous emission (including the fluctuations of momentum carried away by fluorescence photons, as well as the fluctuations due to variations in the number of photons absorbed in each of the laser waves). In the 1D case, the corresponding diffusion coefficient $\mathcal{D}_p'$ is smaller than $\mathcal{D}_p''$ by the ratio $(\Gamma/\Delta)^2$. However, $\mathcal{D}_p'$ is not expected to depend on the volume of the lattice cell, so that for a unit cell of large dimensions this term may become larger than $\mathcal{D}_p''$. As a result, the temperature may increase when the length scale of the lattice becomes too large.

[25] Michael M. Burns, Jean-Marc Fournier, and Jene A. Golovchenko, Phys. Rev. Lett. **63**, 1233 (1989).

[26] One should note, however, that the optical potential is spatially modulated along lines parallel to Oz besides those given by Eq. (A3).

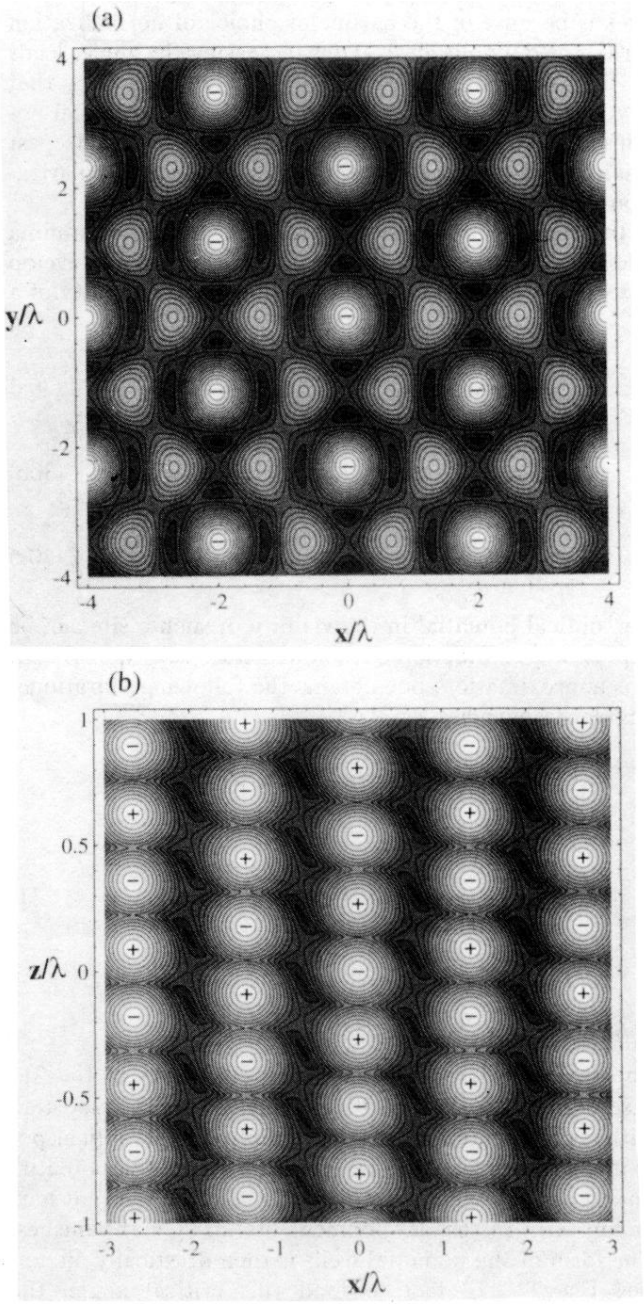

FIG. 10. Topography of the optical potential for the umbrellalike configuration discussed in Sec. III B 3. (a) Section in the plane $z=0$. The potential minima are on a 2D hexagonal lattice. (b) Section of the potential in the plane $y=0$. Here too the relationship to the initial 1D configuration persists along lines parallel to Oz. The form of the 3D optical lattice is shown in Fig. 3.

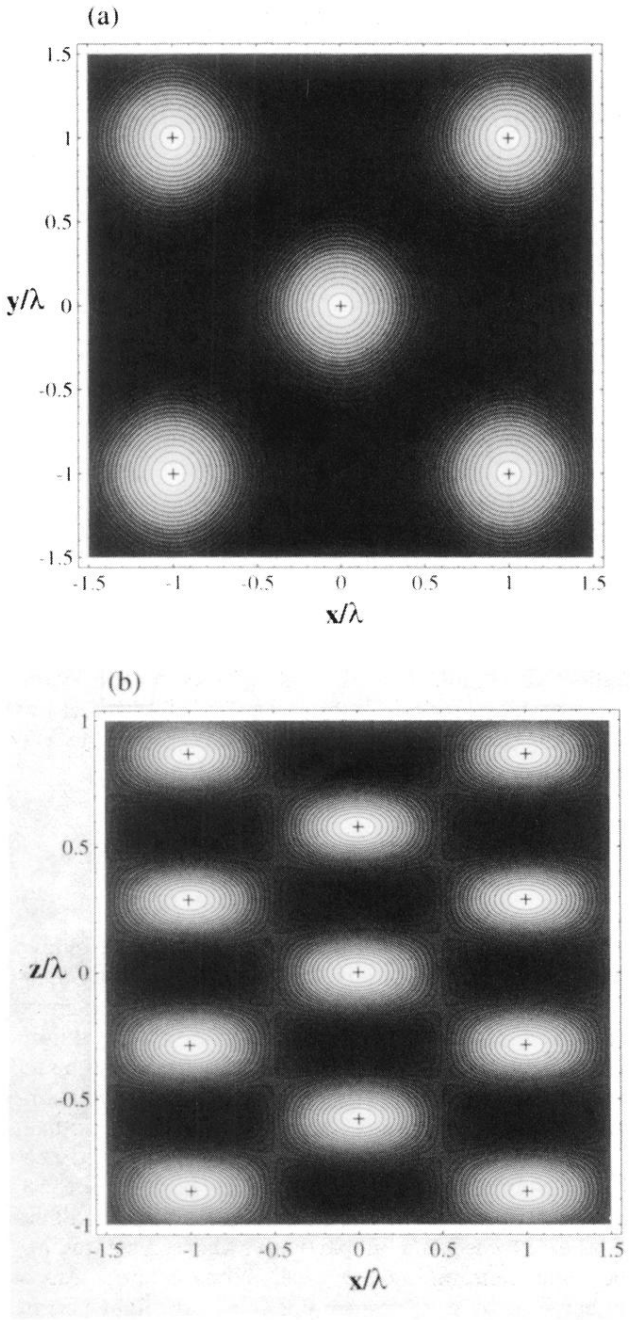

FIG. 11. Optical potential in the case of the 3D configuration proposed in Sec. IV for $\theta_x = \theta_y = 30°$. The optical lattice has the same symmetry as the one considered in Sec. III B 1 (see Fig. 4), but the basis here consists of a single potential well (instead of two wells associated with opposite circular polarizations of light; see Fig. 4). The lattice is therefore ferromagnetic. Totally dark zones in the figure indicate regions where the light intensity is vanishing. (a) Section in the xOy plane ($z = 0$). (b) Section in the xOz plane ($y = 0$).

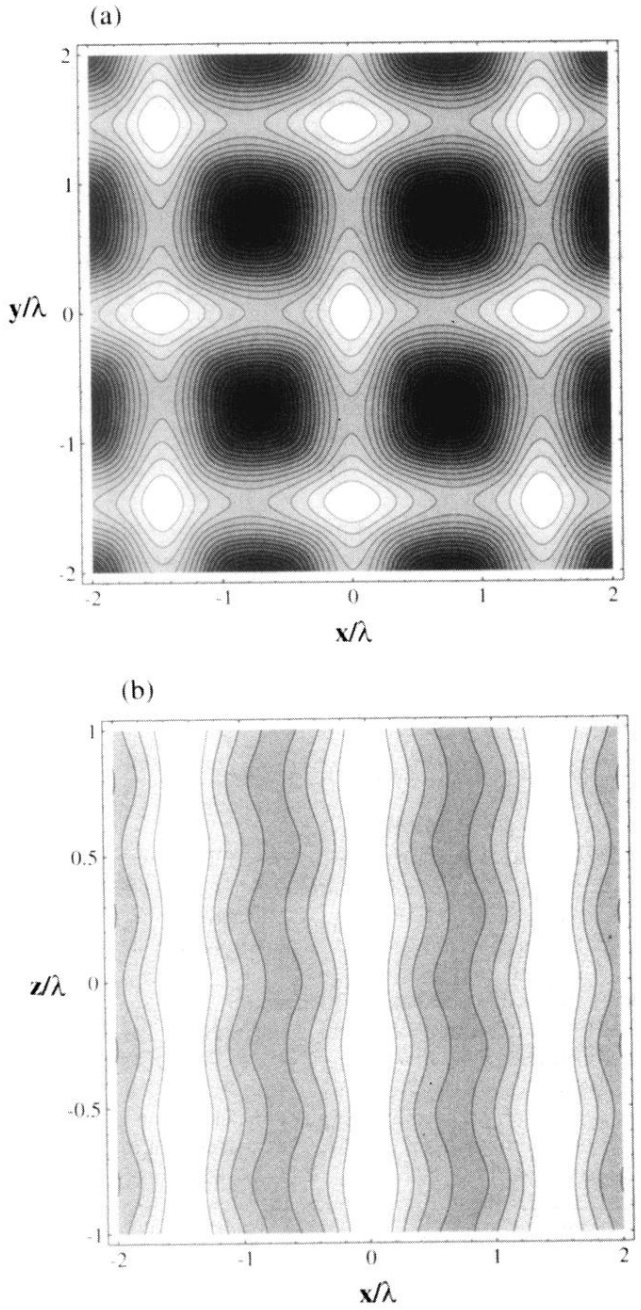

FIG. 12. Potential map for the generalization of the σ^+-σ^- configuration for $\theta_x = \theta_y = \theta = 20°$. (a) Section in the plane $z = 0$. The optical potential minima are located on a square lattice in this plane. The light polarization is linear at these sites. (b) Section in the plane $y = 0$. *Wires* of minimum potential (white lines) are present. The light polarization forms a helix of pitch $\lambda_+/4$ as an atom moves along these lines.

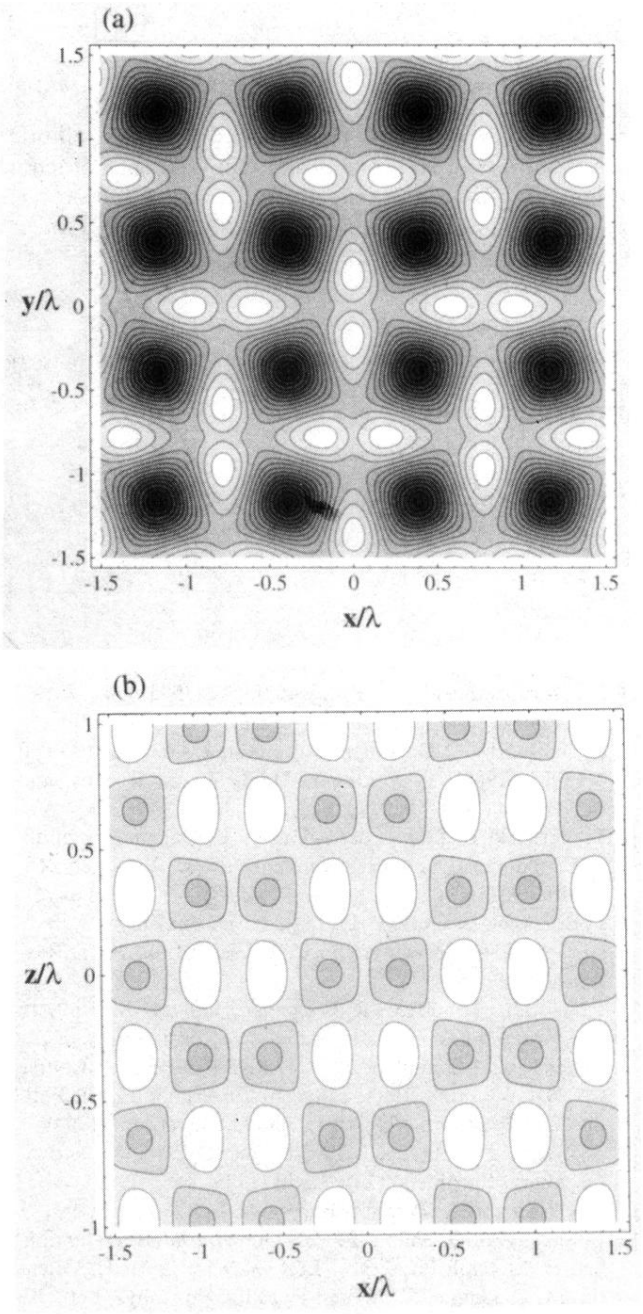

FIG. 13. Sections of the optical potential in the (a) xOy and (b) xOz planes for $\theta_x = \theta_y = \theta = 40°$. As the angle θ has a value which is larger than the critical value, the topography of the potential is significantly modified. In particular, the wires of minimum potential along Oz disappear.

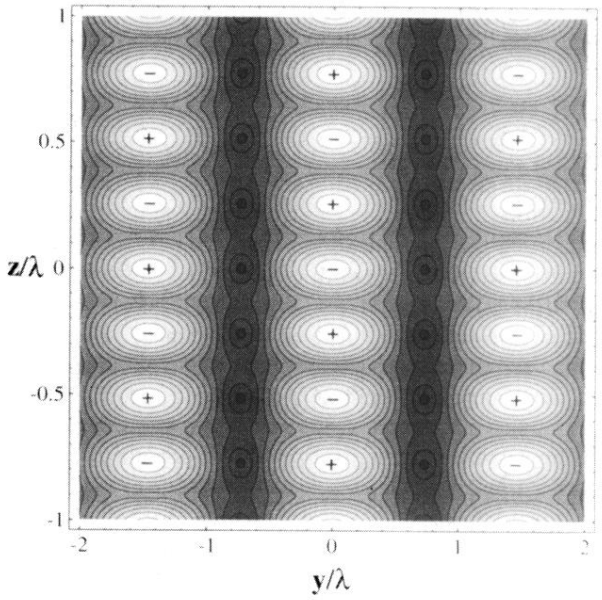

FIG. 5. Topography of the optical potential for the case of the 2D generalization of the lin⊥lin configuration presented in Sec. III A. The minima of the optical potential (associated with larger light shifts) are represented by the lightest zones of the figure. The sign of the circular polarization inside the potential wells is given. Atoms are expected to be localized inside the potential wells, which are regularly distributed on a lattice of the type presented in Fig. 2(a). Darker zones correspond to local maxima of the optical potential.

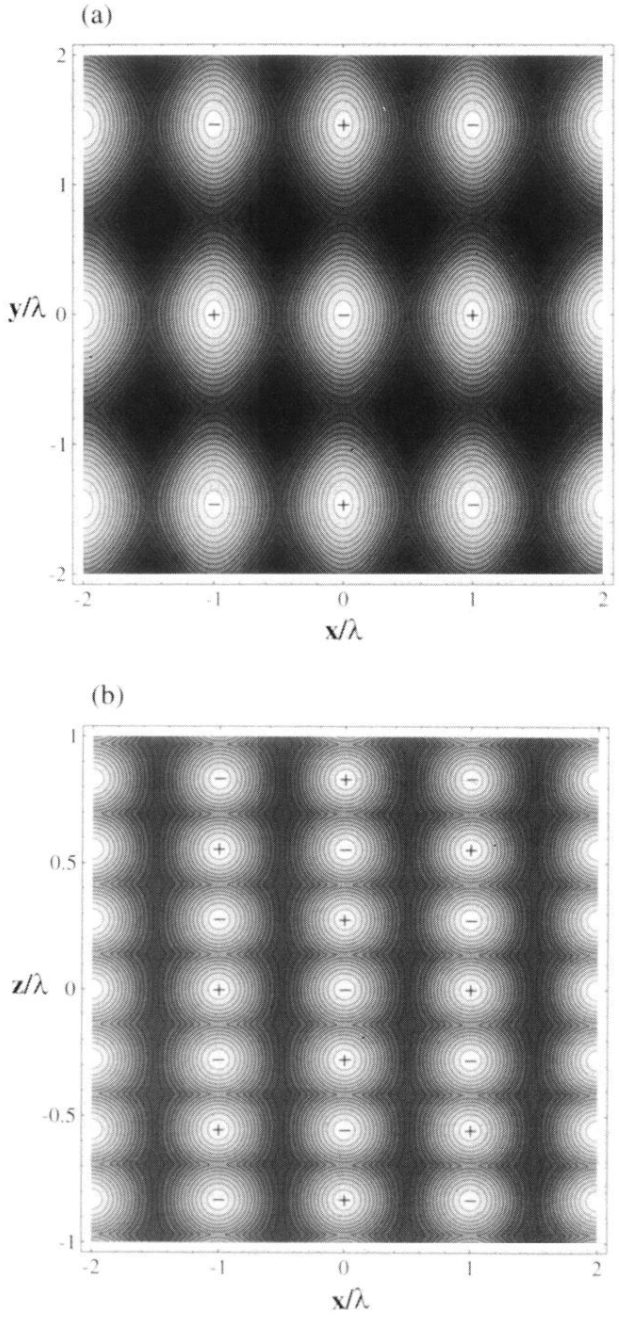

FIG. 6. Optical potential map for the 3D configuration of Sec. III B 1 in the particular case where $\theta_x = 20°$ and $\theta_y = 30°$. The different gray levels correspond to different values of the light shifts, the white zones denoting the potential minima. (a) Section of the potential in the xOy plane ($z = 0$). The projection of the lattice in this plane is very similar to the 2D lattice obtained using two mutually orthogonal standing waves of Refs. [11,22]. Totally dark zones are present, indicating destructive interference between the four cooling beams. (b) Section in the xOz plane ($y = 0$). In this plane, the form of the initial 1D configuration persists along some lines parallel to Oz.

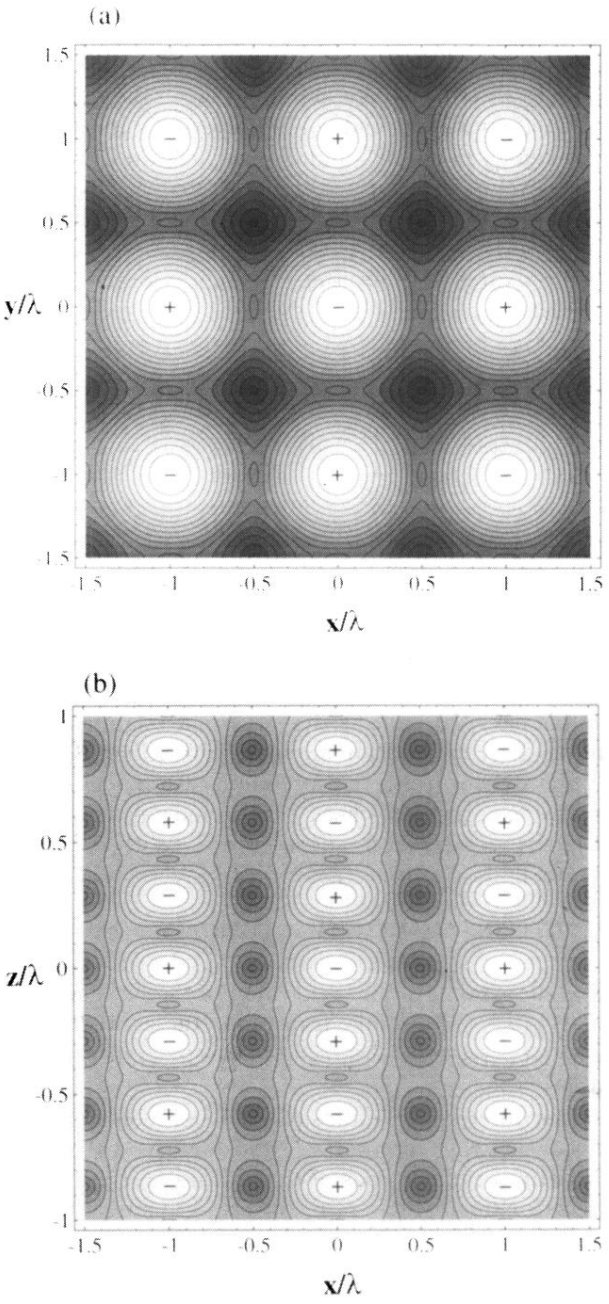

FIG. 7. Optical potential map for the 3D configuration of Sec. III B 2 in the particular case where $\theta_x = \theta_y = 30°$. The different gray levels correspond to different values of the light shifts, the white zones denoting the potential minima. The topography is very similar to the one of Fig. 6 because the two configurations originate from the same 1D situation. Important differences, however, exist due to the presence of π polarized light in the present scheme. (a) Section of the potential in the xOy plane ($z = 0$). Totally dark zones are now absent because of the π polarized light. (b) Section in the xOz plane ($y = 0$).

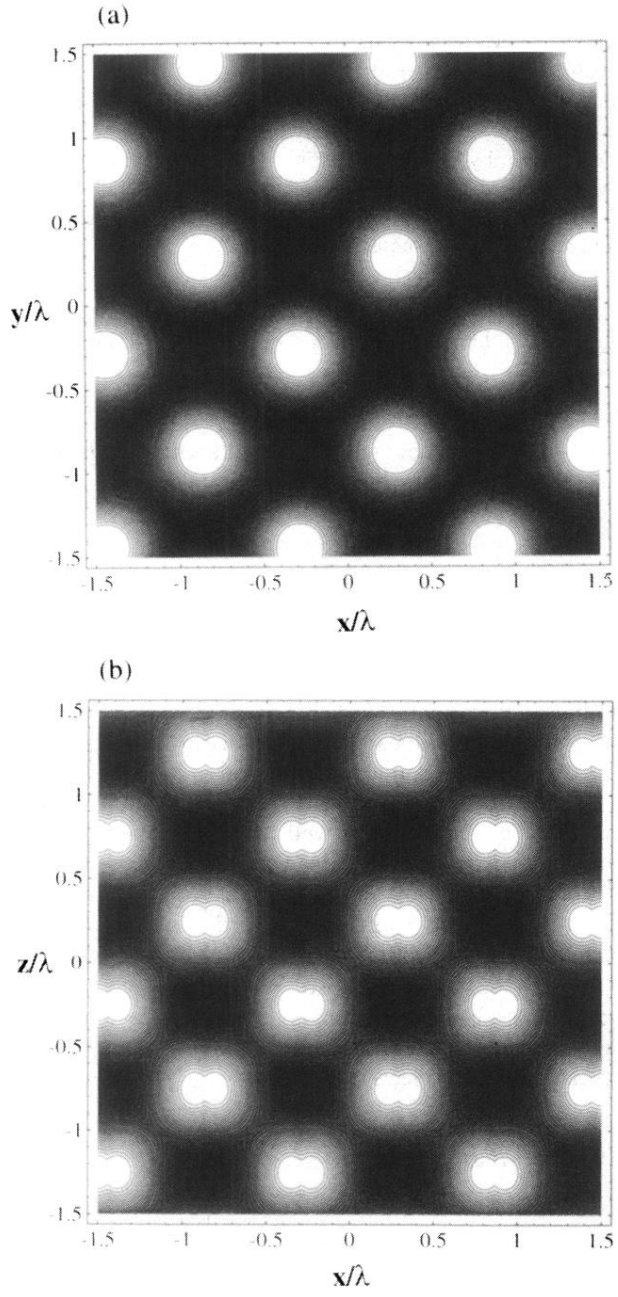

FIG. 9. Potential map for the configuration studied in Sec. III B 2, for $\theta_x = \theta_y = 60°$ (i.e., beyond the critical angle). The minima of the optical potential are now located in regions corresponding to π polarization of the light. (a) Section in the x-y plane ($z = \lambda_+/8$). (b) Section in the x-z plane ($y = \lambda_y/4$).